https://ntrs.nasa.gov/search.jsp?R=19720012672 2020-03-23T11:24:30+00:00Z

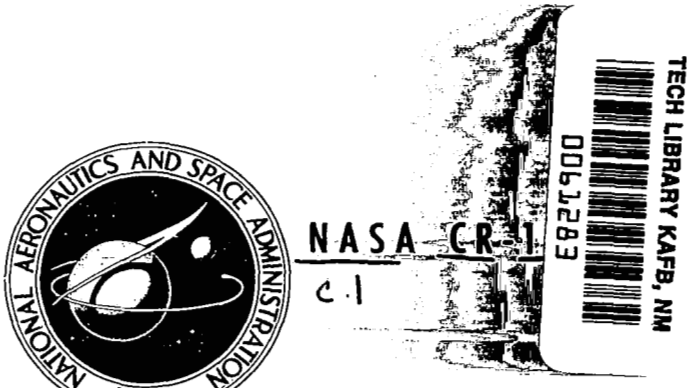

LOAN COPY: RETURN TO
AFWL (DOUL)
KIRTLAND AFB, N. M.

NASA CONTRACTOR REPORT

NASA CR-1985

ADDITIONAL RESEARCH ON INSTABILITIES IN ATMOSPHERIC FLOW SYSTEMS ASSOCIATED WITH CLEAR AIR TURBULENCE

by Richard C. Stoeffler

Prepared by
UNITED AIRCRAFT CORPORATION
East Hartford, Conn.
for

NATIONAL AERONAUTICS AND SPACE ADMINISTRATION • WASHINGTON, D. C. • APRIL 1972

TECH LIBRARY KAFB, NM

0061283

1. Report No.	2. Government Accession No.	3. Recipient's Catalog No.
NASA CR-1985		

4. Title and Subtitle	5. Report Date
ADDITIONAL RESEARCH ON INSTABILITIES IN ATMOSPHERIC FLOW SYSTEMS ASSOCIATED WITH CLEAR AIR TURBULENCE	April 1972
	6. Performing Organization Code

7. Author(s)	8. Performing Organization Report No.
Richard C. Stoeffler	
	10. Work Unit No.

9. Performing Organization Name and Address	11. Contract or Grant No.
UNITED AIRCRAFT CORPORATION East Hartford, Connecticut	NASW-1582
	13. Type of Report and Period Covered
	Contractor Report

12. Sponsoring Agency Name and Address	14. Sponsoring Agency Code
National Aeronautics and Space Administration Washington, D. C. 20546	RAA

15. Supplementary Notes

16. Abstract

Additional analytical and experimental fluid mechanics studies were conducted to investigate instabilities in atmospheric flow systems associated with clear air turbulence.

The experimental portion of the program was conducted using the UARL Open Water Channel which allows investigation of flows having wide ranges of shear and density stratification. The program was primarily directed toward studies of the stability of straight, stratified shear flows with particular emphasis on the effects of velocity profile on stability; on studies of three-dimensional effects on the breakdown region in shear layers; on the interaction of shear flows with long-wavelength internal waves; and on the stability of shear flows consisting of adjacent stable and unstable layers. The results of these studies were used to evaluate methods used in analyses of CAT encounters in the atmosphere involving wave-induced shear layer instabilities of the Kelvin-Helmholtz type.

A computer program was developed for predicting shear-layer instability and CAT induced by mountain waves. This technique predicts specific altitudes and locations where CAT would be expected.

17. Key Words (Suggested by Author(s))	18. Distribution Statement
1. Clear Air Turbulence; ~~Atmospheric Fluid Mechanics~~ 2. Atmospheric turbulence 3 Fluid mechanics 10 Aug 72	Unclassified - Unlimited

19. Security Classif. (of this report)	20. Security Classif. (of this page)	21. No. of Pages	22. Price*
Unclassified	Unclassified	75	$3.00

*For sale by the National Technical Information Service, Springfield, Virginia 22151

FOREWORD

Analytical and experimental fluid mechanics investigations were performed to investigate instabilities in atmospheric flow systems associated with clear air turbulence. This work was a continuation of investigations reported in NASA Contractor Report CR-1604, "Research on Instabilities In Atmospheric Flow Systems Associated With Clear Air Turbulence," by J. W. Clark, R. C. Stoeffler, and P. G. Vogt (June 1970). The program was conducted by United Aircraft Research Laboratories under Contract NASW-1582 with National Aeronautics and Space Administration Headquarters, Washington, D. C., 20546. The program was under the technical direction of the Chief, Aerodynamics and Fluid Dynamics Branch, Code RAA.

TABLE OF CONTENTS

RESULTS AND CONCLUSIONS

1. The water channel experiments to investigate the stability of straight, two-dimensional, stratified shear flows having "S-shaped" velocity profiles confirmed that the shape of the velocity profile affects the dimensionless wavenumber, αd*, of the instabilities which can occur. The values of αd observed in experiments with "S-shaped" profiles were significantly larger than those observed previously in experiments with hyperbolic tangent profiles. This result is in agreement with the theoretical stability criteria of Hazel for "S-shaped" profiles and Drazin for hyperbolic tangent profiles.

2. The experimental results and the theoretical stability criteria for two-dimensional flows were also in good agreement regarding the critical value of Richardson number. Both "S-shaped" and hyperbolic tangent profiles are stable for Richardson numbers greater than 0.25.

3. Although the values of dimensionless wavenumber, αd, at which instabilities occur at a Richardson number of 0.25 are larger for "S-shaped" profiles than for hyperbolic tangent profiles, the actual wavelengths, λ, are about the same (assuming that the shear layer thicknesses, the velocity differences across the shear layer, and the mean shears at the center of the shear layers are approximately equal). The theory indicates that the higher values of αd are due mainly to higher values of the parameter d necessary to describe "S-shaped" profiles. The experimental results tend to confirm this.

4. The preceding conclusion also applies to the wavelengths of instabilities that can be expected when stable shear layers in the atmosphere are destabilized by long-wavelength waves (i.e., wave-induced instabilities), such as mountain lee waves. If the shear-layer thickness, the velocity difference across the shear layer, and the mean shear at the center of the layer are fixed, then the wavelength of the instability occurring when the Richardson number decreases to 0.25 will be about the same, whether the profile is an "S" or a hyperbolic tangent. This wavelength is closely approximated by the wavelength given by Drazin's theory, $\lambda_E = (2\pi/\sqrt{2}) \cdot 2d$, where d is taken as half the shear-layer thickness.

---

*The characteristic breakdown flow pattern of Kelvin-Helmholtz-type instabilities consists of waves which develop into vortices and turbulence. The wavenumber α is $2\pi/\lambda$, where λ is the wavelength of the instability; d is one of several parameters which describe the velocity profile (d is approximately half of the shear-layer thickness for hyperbolic tangent profiles, but this is not a good approximation for "S-shaped" profiles).

5. Water channel experiments and theoretical studies were conducted to investigate the stability of straight, stratified shear flows in which the width of the shear layer was from about 4 to 40 times its thickness. Thus, these shear layers were "three-dimensional" as opposed to the usual two-dimensional shear layer which is assumed to extend uniformly to infinity in the direction transverse to the flow. The results indicate that "three-dimensional" flows are more stable than two-dimensional flows. The measurements also indicate that, although the velocity profiles were significantly different from hyperbolic tangent profiles analyzed by Drazin for two-dimensional flows, the wavelengths of the initial Kelvin-Helmholtz-type instabilities that occur are adequately predicted by his criterion.

6. Shear layer instabilities induced by long-wavelength internal waves were also investigated in water channel experiments. Kelvin-Helmholtz-type waves which grew in amplitude and transitioned to vortices and turbulence were observed in the thin shear layers. These disturbances moved at the mean flow velocity and were superimposed on the stationary long-wavelength internal waves. Occurrence of the instabilities was predicted quite well using the method used previously in this program to predict CAT resulting from shear-layer instabilities induced by mountain lee waves.

7. Water channel experiments were conducted to investigate the stability of combined shear layers consisting of adjacent stable and unstable layers. The results indicated that instability is initiated in the individual unstable layers at wavelengths that would be predicted by theory based on the thickness of these individual unstable layers. However, in the final stages of vortex growth and turbulent breakdown, the wavelength increases to about that which would be predicted based on the thickness of the combined layer. Thus, in combined shear layers, small-amplitude, short-wavelength disturbances associated with initial instabilities in individual layers can result in large-amplitude, long-wavelength disturbances.

8. A method was developed, and included in a computer program, for predicting the occurrence of CAT in mountain waves. The method compares the amplitude of a lee wave required to destabilize an initially stable layer (i.e., to reduce the Richardson number to 0.25) with a predicted lee wave amplitude. The layers are identified using rawinsonde data. Lee wave activity is predicted using the United Air Lines nomogram which is based on the sea level pressure difference between two ground stations and maximum wind velocity associated with the wave zone of interest. Lee wave amplitude is estimated from a correlation of predicted lee wave activity (using the UAL nomogram) with wave amplitudes deduced from reconstructed mountain-wave flow fields. Turbulence is predicted at altitudes where the lee wave amplitudes required for instability are less than the predicted lee wave amplitudes.

INTRODUCTION

The general objectives of the present program were: (1) to gain increased understanding of the nature and causes of turbulent atmospheric phenomena, particularly clear air turbulence; (2) to develop improved criteria for predicting neutrally stable states in atmospheric flow systems; and (3) to compare the results of this research with available meteorological data and attempt correlations.

The results of all fluid mechanics analyses and experiments conducted under this program are reported in Refs. 1 through 5. The initial work (Refs. 1 and 2) provided evidence that long-wavelength waves, such as mountain waves, could destabilize initially stable shear layers which occur in the atmosphere. Since long-wavelength waves may occur quite often in the atmosphere, the breakdown of these layers could account for an appreciable fraction of CAT which is encountered. The present report summarizes further research reported in detail in Refs. 3 through 5. The specific objectives of the latter research were: (1) to conduct further experiments on the effect of the shape of the velocity profile on the stability of straight, two-dimensional, stratified shear flows; (2) to investigate the stability of "three-dimensional" flows by conducting experiments in the UARL Open Water Channel on the stability of straight, stratified shear flows in which the width of the shear layer was less than the width of the channel; (3) to further investigate experimentally the interaction of long-wavelength waves with stable shear layers; and (4) to develop a computer program which predicts shear-layer instability and CAT induced by mountain lee waves. Appendix I contains the derivation of equations used to compare theoretical with experimental "S-shaped" velocity profiles. Appendix II contains a discussion of an investigation of the stability of shear flows consisting of adjacent stable and unstable layers and a description of the method used to obtain a stability criterion for "three-dimensional", straight, stratified shear flows.

STABILITY OF TWO-DIMENSIONAL, STRAIGHT, STRATIFIED SHEAR FLOWS HAVING "S-SHAPED" VELOCITY PROFILES

The primary purpose of this part of the fluid mechanics program was to investigate the effects of the shape of the velocity profile on the stability of straight, two-dimensional, stratified shear flows. First, experiments were conducted to obtain data on the stability of flows having "S-shaped" velocity profiles; these data were also compared with theoretical stability criteria. The results were then compared with results from an earlier investigation of the stability flows having hyperbolic tangent profiles. The program was directed toward three areas: (1) identifying the conditions under which such flows become unstable, (2) determining the characteristics of the flow during the initial phases of breakdown, and (3) evaluating existing theoretical stability criteria for subsequent use in studying atmospheric shear flows.

Review of Two-Dimensional Flows Having Hyperbolic Tangent Profiles

The stability of shear flows having hyperbolic tangent velocity profiles was investigated in detail in earlier work under this program (Refs. 1 through 4). Flows of this type were studied using the UARL Open Water Channel, shown in Fig. 1. This facility provides a 2-ft-wide by 10-ft-long by 12-in.-deep, non-recirculating, open channel flow. Filter beds made from porous foam material are used to introduce desired vertical and transverse velocity profiles in the flow. Hot-water nozzles in the plenum are used to introduce vertical temperature gradients and, hence, density stratification. Dye tracing and hydrogen bubble wire techniques are used for flow visualization and for measurement of the inlet velocity profile; standard submersible mercury thermometers were used to measure temperatures. This facility and its associated instrumentation are described in detail in Refs. 1 and 2.

Velocity profiles approximating hyperbolic tangent profiles were obtained by shaping the foam material in the filter bed as shown in Sketch A. The stability of flows having such profiles was studied theoretically by Drazin (Ref. 6) and others. The hyperbolic tangent velocity profile which most closely approximates the profiles in the channel is given by

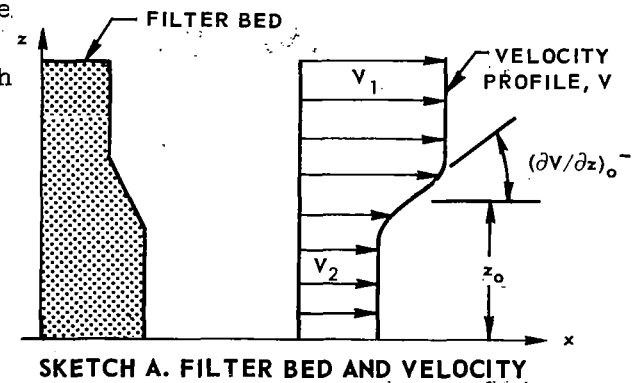

SKETCH A. FILTER BED AND VELOCITY PROFILE FOR HYPERBOLIC TANGENT VELOCITY PROFILE

$$V = V_o + \frac{\Delta V}{2} \cdot \tanh\left(\frac{z - z_o}{d}\right) \tag{1}$$

where V is the local velocity at height z above the channel floor; $V_o = (V_1 + V_2)/2$ is the velocity at the center of the shear layer at height z_o; $\Delta V = (V_1 - V_2)$; and $d = (\Delta V)/2(\partial V/\partial z)_o$. The parameter d is a scale length and is approximately half the thickness of the shear layer. Drazin also used an exponential variation of density with height:

$$\rho/\rho_o = e^{-\beta\left(\frac{z-z_o}{d}\right)} = e^{-\frac{Ri \cdot d \cdot (\partial V/\partial z)_o^2}{g}\left(\frac{z - z_o}{d}\right)} \tag{2}$$

where Ri is the Richardson number and g is the gravitational constant. Since the change in density across the shear layer is small, a good approximation to Eq. (2) is

$$\rho/\rho_o = 1 - \frac{Ri \cdot d \cdot (\partial V/\partial z)_o^2}{g}\left(\frac{z - z_o}{d}\right) \tag{3}$$

Drazin derives a criterion for stability in Ref. 6 by introducing a perturbation stream function

$$\psi' = \phi(z) \cdot e^{i\alpha(x-ct)} \tag{4}$$

into the equations governing the motion of the fluid. Here, α is the wavenumber, $\alpha = 2\pi/\lambda$, and c is the complex wave velocity, $c = c_r + i \cdot c_i$. The equations of motion then yield a single stability equation. Making use of the fact that the perturbations neither amplify nor decay when $c_i = 0$, Drazin solves for the following equation for neutral stability on the αd - Ri plane:

$$\alpha d = \sqrt{\frac{1}{2} \pm \sqrt{\frac{1}{4} - Ri}} \tag{5}$$

Sketch B shows this boundary which separates stable and unstable regions. The criterion indicates that the flow would be stable for disturbances of all dimensionless wavenumbers, αd, for Ri > 0.25. For Ri < 0.25, the flow would be unstable for dimensionless wavenumbers which lie inside the boundary and a Kelvin-Helmholtz (K-H) type of instability would occur.

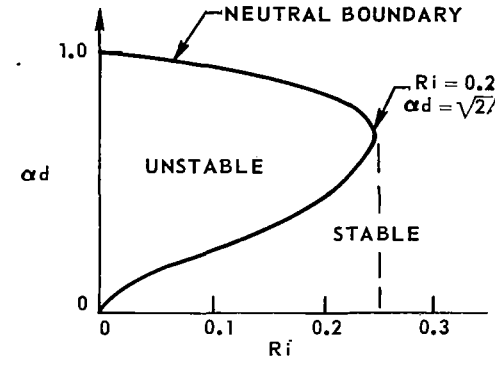

SKETCH B. DRAZIN'S NEUTRAL STABILITY BOUNDARY FOR HYPERBOLIC TANGENT PROFILES

The results of UARL Open Water Channel investigations of the stability of flows having hyperbolic tangent velocity profiles are summarized and compared with Drazin's theoretical criterion in Fig. 2. For each flow condition, the Richardson number was calculated using the slopes $(\partial V/\partial z)_o$ and $\partial T/\partial z$ from the measured profiles. The scale length, d, was calculated using the slope $(\partial V/\partial z)_o$ and the velocity difference ΔV from the velocity profile; ΔV was based on the maximum and minimum velocities in the vicinity of the edges of the shear layer. The wavenumber, $\alpha = 2\pi/\lambda$, of instabilities observed in the shear layer was calculated using wavelengths determined from photographs of dye traces. Thus, each flow condition at which waves were observed is identified by a point on the plot of αd vs Ri.

The symbols in Fig. 2 denote different flow characteristics that were observed. The open circle symbols denote conditions at which only Kelvin-Helmholtz-type waves were observed in the shear layer; that is, the waves extended the entire length of the channel without breaking down. The wavelengths of these waves ranged from about 3 to 6 in. The open circle symbols with flags indicate the nature of the disturbances observed --- for example, small-amplitude waves which persisted, waves which seemed to grow in amplitude to a certain point and then not grow further as they progressed downstream, and waves which appeared in the flow only intermittently. The half-solid symbols denote flow conditions in which the waves transitioned to vortices but did not transition to turbulence before reaching the downstream end of the channel. The full-solid symbols denote flow conditions at which the full sequence of events associated with complete shear-layer breakdown occurred --- waves, vortices, and turbulence. The crosses indicate conditions at which no waves of the type associated with instability occurred.

Examination of Fig. 2 indicates that most of the observations are in good agreement with Drazin's boundary. All cases in which full transition was observed fall in the unstable region. Six cases in which waves were observed fall in the stable region. The intermittent small-amplitude waves indicated at Ri = 0.43 and steady small-amplitude waves at Ri = 0.38 were unexpected; in subsequent tests at approximately the same conditions, no waves were observed. Four cases were observed which fall above the boundary but at Ri < 0.25. These four cases were, at the time of the tests, suspected to be attributable to differences between the experimental velocity profile and Drazin's hyperbolic tangent profile. This hypothesis was based on a theoretical study by Hazel (Ref. 7) which showed that instabilities associated with flows having "S-shaped" velocity profiles could have dimensionless wavenumbers greater than 1.0.

Stability Criteria of Hazel for "S-Shaped" Velocity Profiles

"S-shaped" velocity profiles are developed in the Water Channel by shaping the porous foam filter bed as shown in Sketch C.

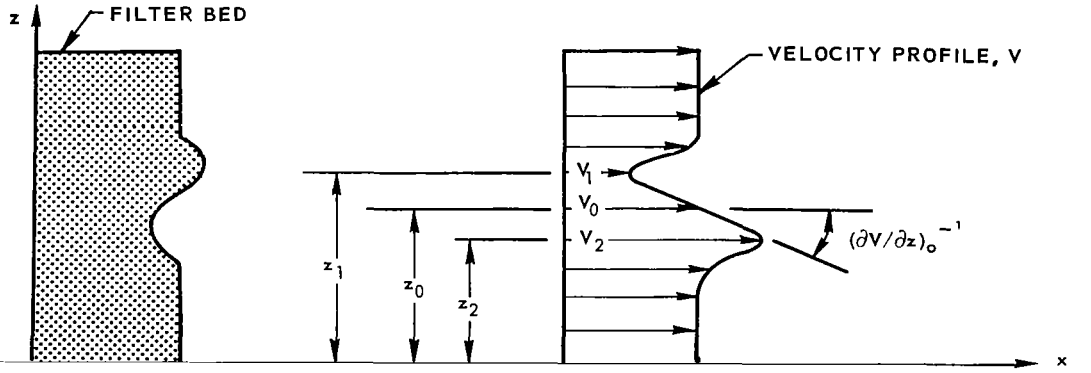

SKETCH C. FILTER BED AND VELOCITY PROFILE FOR "S-SHAPED" VELOCITY PROFILE

The velocity profile used by Hazel in this theoretical study is

$$V = V_0 + \frac{\Delta V}{2} \cdot \operatorname{sech}^b \left(\frac{z - z_o}{d}\right) \cdot \tanh \left(\frac{z - z_o}{d}\right) \qquad (6)$$

where b is an exponent that affects the shape of the "S" and, as before, $d = (\Delta V)/2(\partial V/\partial z)_o$. The relationship of the velocity difference ΔV to $(V_1 - V_2)$ and b is (see derivation in Appendix I)

$$\Delta V = (b+1)^{\frac{b+1}{2}} \cdot b^{-\frac{b}{2}} (V_1 - V_2) \tag{7}$$

The theoretical density profile used by Hazel is

$$\rho = \rho_o \, e^{-\frac{Ri \cdot d \cdot (\partial V/\partial z)_o^2}{g}} \cdot \tanh\left(\frac{z - z_o}{d}\right) \tag{8}$$

Hazel derives criteria for stability in Ref. 7 for several velocity and density profiles. This is done by solving (using numerical techniques) a differential equation which is satisfied by one Fourier component of the velocity perturbation for a plane, two-dimensional, Boussinesq shear flow. The full perturbation velocity is given by

$$w(x,z,t) = \int_{-\infty}^{\infty} w(z) \, e^{i\alpha(x-ct)} \cdot d\alpha \tag{9}$$

Like Drazin's criterion, Hazel's criteria (see Sketch D) indicate that the flow would be stable for disturbances of all dimensionless wavenumbers for Ri > 0.25. For Ri < 0.25, the flow would be unstable for dimensionless wavenumbers which lie inside the boundaries. The locations of the neutral stability curves on the αd - Ri plane are dependent upon the value of the exponent b (see sketch).

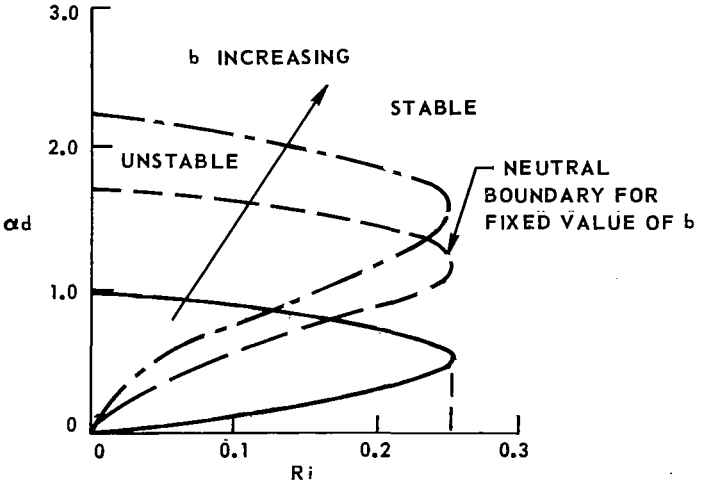

SKETCH D. HAZEL'S NEUTRAL STABILITY BOUNDARIES FOR "S-SHAPED" PROFILES

Summary of Experiments with "S-Shaped" Velocity Profiles

Characteristics of Breakdown of Flow

Figure 3 illustrates the stages observed as the flow in the shear layer breaks down. The breakdown characteristics were very similar to those for hyperbolic-tangent-type flows. There are four very distinct and repeatable stages which occur. The photographs in Fig. 3 were taken through the lucite channel side wall with the flow from left to right. The scale in the photographs was in the flow close to the dye traces.

In Fig. 3(a), the flow appears undisturbed. In Fig. 3(b), 28 in. further downstream, the center dye trace indicates the presence of a K-H wave amplifying as it progresses downstream. The wave has a wavelength of about $\lambda = 5$ in. and an amplitude (half the distance from trough to crest) of about $a = 0.25$ in. at this point. By placing dye traces at several transverse locations across the channel, it was verified that the flow was approximately two-dimensional, i.e., the wave extended across the channel. In Fig. 3(c), another 24 in. downstream, the waves have rolled up into vortices. The circulation of the vortices has the same sense as the vorticity introduced by the shear --- the shear is negative in this flow condition, and all of the vortices rotated counterclockwise. These vortices grew slightly in size as they drifted downstream. Their downstream drift velocity was approximately V_o, the velocity upstream at the center of the shear layer. The flow was also two-dimensional at this stage. In Fig. 3(d), another 10 in. downstream --- 70 in. downstream of the filter bed --- the vortices have "burst" and the flow appears turbulent. The fluid motions were three-dimensional at this stage.

Velocity, Temperature, and Density Profiles

Velocity, temperature, and density profiles for three flow conditions are shown in Fig. 4. These data are for three different Richardson numbers and three different values of the exponent b used in Hazel's theoretical velocity profile. The corresponding velocity and density profiles in Hazel's theory are shown by the dashed lines. Once a velocity profile had been measured, the value of the exponent b was derived so as to provide a reasonably good match between theoretical and experimental velocity profiles. The theoretical profile was chosen by matching to the data the following (see Appendix I and Sketch C): (1) the velocity difference, $V_1 - V_2$, (2) the vertical distance between V_1 and V_2, $z_1 - z_2$, and (3) the mean velocity gradient, $(\partial V/\partial z)_o$, at z_o. The corresponding theoretical density profile was chosen by matching the density gradient and mean density of the experimental profile at the center of the shear region.

Comparison of Experimental Results with Hazel's Theoretical Stability Criteria

Figure 5 is a summary of the results and a comparison with Hazel's theoretical criteria. As in Fig. 2, the symbols denote different flow characteristics that were observed. The values of the exponent b which provide the best match between the theoretical and experimental velocity profiles are given next to the symbols.

Most of the experimental results are in agreement with Hazel's stability boundaries. For all cases in which instability was observed, the Richardson number was less than 0.25, and only one stable case was observed for which the Richardson number was less than 0.25 ($\alpha d = 0$, Ri = 0.2). For all but one of the cases for which instability was observed, the dimensionless wavenumbers, αd, were greater than 1.2. This is in contrast to the results obtained for hyperbolic tangent velocity profiles (see Fig. 2) where the αd's associated with instabilities were less than 1.2 for all but one case.

Hazel's theory shows that as the value of b increases, the range of wavenumbers, αd, of instabilities which can occur also increases. The data appear to confirm this trend, although insufficient data were obtained to make detailed comparisons with Hazel's criteria for low values of b. Only two cases are not in agreement with Hazel's neutral stability boundaries. They are (1) Ri = 0, $\alpha d = 2.4$, b = 0.8, and (2) Ri = 0, $\alpha d = 2.07$, b = 0.3. However, these values of b are questionable since the agreement between the theoretical and experimental velocity and density profiles was comparatively poor for these cases.

Concluding Remarks

The most important result of these experiments is that the data provide sufficient evidence to confirm the hypothesis that instabilities which occur in flows having "S" profiles generally have values of αd considerably larger than those in flows having hyperbolic tangent profiles. As explained below, however, the actual wavelengths of instabilities at Ri = 0.25 are about the same due to compensating changes in d.

The theoretical criteria of Hazel differ from Drazin's criterion only in that one might expect to observe instabilities having larger dimensionless wavenumbers in unstable shear layers with "S" profiles. Therefore, one might be inclined to expect shorter wavelengths for instabilities associated with "S" profiles than with hyperbolic tangent profiles. However, it can be shown that for an experimental velocity profile having a maximum velocity V_1 at z_1, a minimum velocity V_2 at z_2, and a velocity gradient $(\partial V/\partial z)_o$ at the center of the shear layer, the wavelength, λ, at Ri = 0.25 for the best fitting "S" profile is generally about the same as that for the tanh profile. This is because the value of d for the best fitting "S" profile

is larger than that for the tanh profile. Thus, the increase in the critical value of αd is primarily due to an increase in d and, therefore, the wavelengths of instabilities in flows having "S" profiles are approximately the same as those for hyperbolic tangent profiles. This is illustrated in Sketch E which shows, for instabilities associated with αd at Ri = 0.25, the theoretical variation of the ratio of λ for "S-shaped" profiles to λ for hyperbolic tangent profiles with the parameter b (b is related to $z_1 - z_2$, $V_1 - V_2$, and $(\partial V/\partial z)_o$ in Eq. (25) in Appendix I). For the range of b shown, and for b not near zero, this ratio is not greatly different from 1.0. Data from the water channel obtained near Richardson number of 0.25 tend to confirm this:

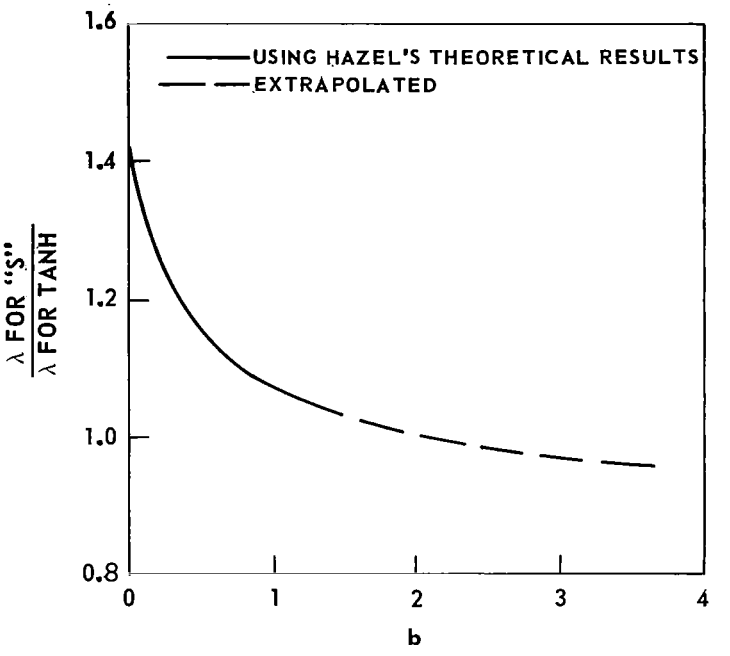

SKETCH E. THEORETICAL RATIO OF WAVELENGTHS FOR Ri = 0.25 FOR "S-SHAPED" AND HYPERBOLIC TANGENT PROFILES

Profile	b	Ri	αd	d, in.	λ, in.
"S-Shaped"	>2.0	0.17	1.8	1.5	5
"S-Shaped"	>2.0	0.16	1.9	1.6	5
Tanh	-	0.24	0.74	0.58	5
Tanh	-	0.16	0.84	0.52	4
Tanh	-	0.12	0.70	0.44	4

As a result, Drazin's value of $\lambda = (2\pi/\sqrt{2})\cdot 2d$ (Fig. 2), where d is approximately equal to half the shear-layer thickness, would provide reasonably good estimates of the wavelengths that might occur in the atmosphere regardless of whether the profiles are "S" or tanh in shape.

The experiments and theories also provide further evidence that 0.25 should be used as the critical Richardson number, and that several distinct waves might be observed in the isentropes when instabilities occur in atmospheric shear layers.

STABILITY OF "THREE-DIMENSIONAL", STRAIGHT, STRATIFIED SHEAR FLOWS

A theoretical criterion for predicting the stability of "three-dimensional", straight, stratified, shear flows is apparently not available. Because the magnitude of the task of developing rigorous theoretical criteria was beyond the scope of this program, a simple analysis based on energy considerations (similar to a method used by Chandrasekhar; Ref. 8) was made; see Appendix II. Criteria obtained using such simple techniques are admittedly questionable and may not be too significant. However, the criterion which was obtained was in qualitative agreement with experimental results. The analysis in Appendix II predicts that the critical Richardson number for "three-dimensional" stratified shear flow is 0.125.

A photograph of a shaped filter bed of the type used to develop velocity profiles in experiments in the Water Channel is shown in Fig. 6. The filter provided no velocity gradient (i.e., the same velocity at all heights above the channel floor) across the 2-ft width of the channel except for a section in the center of the channel span where a hyperbolic tangent vertical velocity gradient was provided. The spanwise distance allowed for transition from hyperbolic tangent velocity gradient to zero velocity gradient was large enough so that horizontal velocity gradients were very small compared with the vertical gradients.

Summary of Experiments with "Three-Dimensional" Flows

Characteristics of Breakdown of Flow

The four distinct and repeatable stages which occurred during breakdown of the "three-dimensional" flows were similar to those observed in tests of two-dimensional flows having hyperbolic tangent and "S-shaped" velocity profiles. Dye traces illustrating the phenomenon are shown in the sketch and in photographs in Fig. 7. At the location in Figs. 7(a) through 7(c), dye from probes at several transverse locations indicated that the disturbance was confined to the flow containing the shear layer in the central portion of the channel. At the location in Fig. 7(d), the vortices have "burst" and the flow appears turbulent. Downstream of this location the turbulence began to spread transversely.

Velocity, Temperature, and Density Profiles

Velocity, temperature, and density profiles are shown in Fig. 8 for three different values of Richardson number. It was found that neither a hyperbolic tangent nor an "S-shaped" profile was particularly representative of the experimental velocity profiles. The temperature and density gradients shown in Fig. 8(b) and (c) indicate that the temperature and density varied approximately linearly through the thermocline which separated the two regions of the flow having approximately uniform temperatures.

Comparison of Results with Theoretical Stability Criterion for Two-Dimensional Flows

Figures 9 through 11 present a comparison of the test results with Drazin's criterion for two-dimensional flows. The data were obtained for three different ranges of shear layer width, w, to thickness, $(2d)_m$, ratios. See Fig. 6 for w. During these tests, w_s in Fig. 6 was varied between 0 and 12 in., and w_t between 2 and 5 in. The shear layer thickness $(2d)_m$ was the measured distance between the maximum and minimum velocities of the shear layer and for most cases was approximately equal to twice the scale length, d. Data was presented in Figs. 9, 10, and 11 for $w/(2d)_m$ between 4.8 and 8.6, 9.7, and 14.3, and 14.5 and 40, respectively.

Except for five cases (all on Fig. 9), the dimensionless wavenumbers for cases where instability was observed are in agreement with Drazin's stability criterion for two-dimensional flows having hyperbolic tangent velocity profiles (i.e., the data points are inside the stability boundary). For the five exceptions the dimensionless wavenumbers were greater than 1.0. This is not unexpected since the velocity profiles were somewhat "S-shaped".

By inspecting Figs. 9 through 11 it can be seen that as the width of the layer containing the vertical velocity gradient decreases, the Richardson numbers at which stable flows are observed generally decrease, and the Richardson numbers above which instabilities are not observed also generally decrease. It appears, then, that the critical Richardson number decreases as the width of the vertical velocity gradient decreases. This trend is shown by the shaded boundary in Fig. 12. The trend is compatible with the result obtained by extending Chandrasekhar's technique for predicting the stability of two-dimensional stratified, shear flows to "three-dimensional" flows (see Appendix II); i.e., the simplified extension of the theory predicts that the critical Richardson number, Ri, for "three-dimensional" flows is 0.125.

Concluding Remarks

The most important result is that data and theory provide evidence that "three-dimensional" stratified shear flows are more stable than two-dimensional flows. The critical Richardson number is less than 0.25; it decreases with decreasing shear layer width to thickness ratios. The results also indicate that, although the experimental velocity and density profiles were quite different from theoretical profiles used by Drazin in his analysis, Drazin's criterion for predicting the wavelength of instabilities in two-dimensional flows could be used to predict the wavelength of instabilities in "three-dimensional" flows. Finally, as many as four or five wavelengths were often observed upstream of the first discernable vortex, as in two-dimensional flows; thus, it is reasonable to expect that several waves will also be observed in isentropes when instabilities occur in "three-dimensional" atmospheric shear layers.

INTERACTION OF LONG-WAVELENGTH WAVES WITH TWO-DIMENSIONAL, STRAIGHT, STRATIFIED SHEAR FLOWS

The primary purpose of this part of the fluid mechanics program was to investigate, using the Water Channel, the destabilization of initially stable shear flows by long-wavelength waves. Evidence that this phenomenon occurs in the atmosphere and may be the cause of an appreciable fraction of clear air turbulence has been documented previously under this program (Refs. 1 through 4). In Ref. 1, an analytical technique was developed to predict when long-wavelength waves, such as mountain lee waves, would destabilize initially stable shear layers in the atmosphere. In using the technique, Ri = 0.25 was used as the critical Richardson number for neutral stability. The increment in shear induced by the presence of long waves was estimated using an extension of a theory developed by Phillips (Ref. 9) and the long-wave wavelenths were estimated using Haurwitz' theory (Ref. 10).

The objectives of the Water Channel experiments and analyses reported in this section were: (1) to investigate the conditions for wave-induced instability and the nature of the initial disturbances, (2) to obtain experimental verification of Phillips' and Haurwitz' theories, and (3) to verify the validity of the combined theoretical approach developed to predict the occurrence of wave-induced shear-layer instabilities.

Theory for Wave-Induced Shear-Layer Instabilities

In Ref. 9, Phillips derives an equation for the increment in shear induced by the presence of a wave traveling along the thermocline in a fluid. The expression he obtained for the wave-induced shear is

$$\Delta(\partial V/\partial z) = (N_M^2 - n^2)\cdot\left(\frac{a}{V_o}\right) \tag{10}$$

where

N_M = Brunt-Väisälä Frequency = $\sqrt{-\frac{g}{\rho}\left(\frac{\partial \rho}{\partial z}\right)}$

n = Wave Frequency = $2\pi V_o/\lambda_{LW}$

a = Wave amplitude

V_o = Wave velocity

For stationary waves, the wave velocity, V_o, is equal to the mean velocity through the wave.

In Ref. 10, Haurwitz derives an expression for the wavelength of waves traveling on a discontinuity of density and velocity at a velocity equal to the mean flow velocity and in a direction opposite to the flow direction (thus, the wave is stationary relative to the observer). The velocity and density gradients were considered to be zero on either side of the discontinuity. The expression obtained by Haurwitz is

$$\lambda_{LW} = \frac{2\pi}{g} \frac{\rho_2 V_2^2}{(\rho_2 - \rho_1)} \left(\left(\frac{V_1}{V_2} \right)^2 \frac{\rho_1}{\rho_2} + 1 \right) \tag{11}$$

where V_1 and ρ_1 are the velocity and density, respectively, of the light fluid which flows over the heavy fluid having a velocity and density V_2 and ρ_2, respectively.

Using estimated values of wave-induced shear, it is possible to predict the effects of long-wavelength waves on local Richardson number in shear flows in the Water Channel (this was done for atmospheric flows in Ref. 1). A schematic diagram of the flow condition is shown in Fig. 13(a). At the left are shown upstream velocity and temperature profiles with a stable shear layer having a thickness 2d. Within this layer, the mean velocity is V_o and the mean temperature is T_o; the mean shear is $(\partial V/\partial z)_o$ (all mean values are at the center of the shear layer).

At the right in Fig. 13(a) is shown a portion of a long-wavelength wave having an amplitude (which might be 0.1 to 4.0 in.) and a wavelength λ_{LW} (which might be 6 to 30 in.). It is assumed in this analysis that the thickness of the shear layer, the mean temperature, and temperature gradient remain constant as the flow within the shear layer experiences the undulating motion.

The minimum local Richardson number in the flow is calculated with the wave-induced shear, $\Delta (\partial V/\partial z)$, added to the initial mean shear. An expression for the minimum Richardson number (which occurs locally at the crest in the example given, but would occur at a trough if the initial shear were negative) is

$$Ri_{MIN} = \frac{N_M^2}{\left(\left| (\partial V/\partial z)_o \right| + \left| \Delta (\partial V/\partial z) \right| \right)^2} \tag{12}$$

Using Eq. (10) for the wave-induced shear, this becomes

$$Ri_{MIN} = \frac{N_M^2}{\left(\left| (\partial V/\partial z)_o \right| + (N_M^2 - n^2)(a/V_o) \right)^2} \tag{13}$$

From Eq. (13) it can be seen that small values of Ri_{MIN} are associated with large initial shears, $(\partial V/\partial z)_o$; with large wave amplitudes, a; with small flow velocities, V_o; and with long wavelengths, $\lambda_{LW}(n = 2\pi V_o/\lambda_{LW})$. The effect of the temperature gradient, $\partial T/\partial z$, on Ri_{MIN} can be seen in Fig. 13(b). With increasing initial temperature gradient, Ri_{MIN} first increases to a maximum value, and then decreases. Since the flow is unstable for $Ri < 0.25$, weakly stabilized layers ($\partial T/\partial z$ near zero) as well as very strongly stabilized shear layers ($\partial T/\partial z$ large) could be destabilized in the presence of a long-wavelength wave.

The dashed curves in Fig. 13(b) were obtained by assuming that $\lambda_{LW} = \infty$, so that $N_M^2 \gg n^2$. This reduces Eq. (10) to

$$\Delta(\partial V/\partial z) = N_M^2 \left(\frac{a}{V_o}\right) \tag{14}$$

The solid curves in Fig. 13(b) were obtained by using the equation for finite wavelength waves, Eq. (10). A comparison of the dashed and solid curves shows (1) that for the flow and wave conditions of Fig. 13(b), use of the simple expression for wave shear, Eq. (14), in the calculation of Ri_{MIN} does not cause large errors in Ri_{MIN}, and (2) that these small errors in Ri_{MIN} which do occur decrease with increasing value of initial shear and are least for very small and very large initial temperature gradients.

Summary of Wave-Induced Shear Layer Instability Experiments

Example of Effects of Long-Wavelength Wave on Local Richardson Number

A long-wavelength wave typical of those studied in the Water Channel is shown in Fig. 14 (λ_{LW} = 14 in. and a = 1.4 in.). The stationary gravity wave is represented by the solid wavy line in the sketch at the top of Fig. 14. A wave-induced instability is represented by the dashed line superimposed on the gravity wave. The wave-induced instability first became apparent as a small amplitude wave just upstream from the trough at x = 7 in. This wave then grows in amplitude, rolling up into vortices near the first crest at x = 14 in. The vortices subsequently transition to turbulence downstream from the crest at x = 14 in. Further downstream (x greater than approximately 30 in.) the turbulence appears to decay and the flow restratifies. Photographs of examples of instabilities which were observed are shown in Fig. 15 (discussed subsequently).

The mean velocities, V_o, measured at the center of the shear layer through the trough and crest were approximately 0.08 and 0.06 ft/sec, respectively --- the average being 0.07 ft/sec (velocity, temperature, and density profiles for this test are shown in Fig. 16). Based on an average of the local flow conditions (measured at the center of the shear layer) at the trough at x = 7 in. and at the crest at x = 14 in., the initial shear, $(\partial V/\partial z)_o$, was -0.71 sec^{-1}, the initial Richardson number, Ri_o, was 0.70, and the wave-induced shear, $\Delta(\partial V/\partial z)$, was -0.32 sec^{-1}. The data of Figs. 16(a) and 16(b) show that the magnitude of the shear was greater at the trough than at the crest. The minimum Richardson number, Ri_{MIN}, was 0.37 and occurred at the trough. This was 53 percent of the initial Richardson number but was greater than the minimum Richardson number for instability, Ri = 0.25. One possible explanation for this discrepancy is that the velocity profile was distorted at the time of its measurement by the wave-induced instabilities which were first apparent just upstream from the trough at x = 7 in. Attempts were made to measure the velocity profile at times when the profile was least disturbed, i.e., between crests and troughs of the wave-induced instabilities. In most other tests in which wave-induced instabilities were observed the minimum Richardson numbers were less than 0.25. The Richardson number which was observed at the crest at x = 14 in., Ri = 1.8, was 260 percent of the initial Richardson number.

Example of Instability Induced by Long-Wavelength Wave

Photographs of an instability induced by a long-wavelength gravity wave are shown in Fig. 15. The upper dye traces show the instability superimposed on the stationary gravity wave. The estimated shape of the undisturbed gravity wave is sketched in white on the photograph. The lower trace appears to be undisturbed by the wave instability. The photographs presented in Fig. 15(b) show that the waves have transitioned to vortices, and the trace in the photograph on the right side of Fig. 15(b) gives evidence that some turbulence exists downstream of the vortices.

Comparison Between Measured and Predicted Wave Shears in Long-Wavelength Waves

Measured values of wave-induced shear caused by long-wavelength waves are compared with values calculated using Phillips' theory (Ref. 9) in Fig. 17. The measured wave shear, $|\Delta(\partial V/\partial z)|$, was determined by taking one-half the difference between the shears at the crest and trough of the long-wavelength wave. The predicted wave shears were calculated using Eq. (10) with measured values of wave amplitude, wavelength, and velocity. The Brunt-Väisälä frequency, N_M, was determined from measured temperature profiles. The results shown in Fig. 17 indicate that in most cases the agreement between measured and predicted values of wave shear was good. The results of these tests provide some experimental evidence that Eq. (10), which is used in this program to predict wave-induced shear in the atmosphere is adequate.

Comparison Between Measured and Predicted Wavelengths of Long-Wavelength Waves

Measured wavelengths of long-wavelength waves are compared with values predicted using Haurwitz' theory (Ref. 10) in Fig. 18. The measured wavelengths, $(\lambda_{LW})_m$, were determined by measuring the distance between crests and troughs of the long-wavelength waves from photographs of the dye traces. The predicted wavelengths, $(\lambda_{LW})_p$, were calculated using Eq. (11) with densities and velocities from measured temperature and velocity profiles, respectively. The data in Fig. 18 indicate only fair agreement between measured and predicted wavelengths. The differences between measured and predicted values increase with increasing wavelength. Part of the reason for this can be seen by examining the equation. One way to increase wavelength, λ_{LW}, is to decrease the density difference, $\rho_2 - \rho_1$. However, this tends to make the predicted wavelengths more sensitive to errors in ρ_1 or ρ_2. This may explain some of the differences in Fig. 18 since in this series of experiments it was easier to obtain changes in λ_{LW} by changing density gradient than velocity gradient. However, this still does not account for the general trend in which the measured wavelengths were generally less than predicted values. Subsequently, the method of Haurwitz (Ref. 10) was examined to determine the possible effect of having a finite depth in the Water Channel on the measured wavelengths. The influence on wavelength of having a free surface above the shear layer and a boundary below the shear layer (applied by Phillips in Ref. 9 to flows in the ocean) was calculated. This method predicted a trend that did not account for the discrepancy in the data. That is, it predicted that wavelength should increase with decreasing depth while the wavelengths measured in the water channel were generally less than those predicted for infinite-depth flows.

Although these differences between theory and experiment at long wavelengths were not resolved, they have no bearing on calculations of atmospheric shear layer instabilities. This will be apparent later in the report.

Prediction of Wave-Induced Shear Instabilities in Water Channel

Figure 19 is a plot of initial shear, $\left|(\partial V/\partial z)_o\right|$, versus the Brunt-Väisälä frequency, N_M. The boundaries define regions where wave-induced instabilities can occur. They were calculated using Eq. (13) with the condition $N_M \gg n$. The boundaries are loci of $Ri_{MIN} = 0.25$ for constant values of a/V_o.

To the left of the boundary for $a/V_o = 0$, the presence of a long-wavelength wave is not required for the flow to be unstable, and any instabilities observed in this region would not be wave-induced. In the region to the right of the boundary for $a/V_o = 0$, the boundaries define the lower limit of a/V_o required for wave-induced instability to occur. For example, a long-wavelength wave having $a/V_o > 0.75$ would cause wave-induced instability to occur anywhere in the region between the boundary for $a/V_o = 0$ and $a/V_o = 0.75$; a long-wavelength wave having $a/V_o < 0.5$ would not cause wave-induced instability anywhere in the region to the right of the boundary for $a/V_o = 0.5$.

The open and solid symbols in Fig. 19 denote cases for which long-wavelength waves were and were not observed, respectively. For each flow condition for which a long-wavelength wave was present (the open symbols) (1) the Brunt-Väisälä frequency was determined from an average of the crest and trough temperature gradients (in these tests, measurements were made at the most upstream crest and trough for which measurements could be made), and (2) the absolute value of initial shear $\left|(\partial V/\partial z)_o\right|$ was determined from an average of the shears measured at the crest and trough. For cases in which long-wavelength waves were not observed (the solid symbols), the Brunt-Väisälä frequency and the absolute value of initial shear were obtained from the temperature gradient and the velocity gradient, respectively, at the center of the shear layer (measurements were made at approximately the same distance downstream from the filter as the measurements that were made when waves were present). The numbers near the symbols denote values of a/V_o. The letters near the symbols denote the type of instability that was observed --- W - wave, V - Vortex, T - Turbulence.

The solid symbols show that long-wavelength waves were not observed in the channel for values of Brunt-Väisälä frequency, N_M, less than about 0.3 sec^{-1}. Therefore, it was not possible to investigate wave-induced instability for values of N_M less than about 0.3 sec^{-1}.

Examination of Fig. 19 indicates that most of the observations are in agreement with the stability boundaries. Instability of some type was observed for all cases which are to be left of the boundary for $a/V_o = 0$. This is expected since the flow is predicted to be unstable in this region even without the additional shear from a long-wavelength wave.

Suspected wave-induced shear instabilities were observed in six tests (see data marked with asterisks) which are to the right of the locus $a/V_o = 0$. In these cases, long-wavelength waves were present. Based on measured values of a/V_o for the six cases for which wave-induced instability was suspected and the values of a/V_o for the cases where wave-induced instability was not observed, the data agree with the stability boundaries.

Concluding Remarks

These laboratory experiments tend to confirm the analytical methods that have been used to estimate wave-induced shear and to predict the onset of shear-layer instabilities in analyses of CAT encounters in the atmosphere. The most important results are shown in Figs. 17 and 19.

Figure 17 shows that the wave shear $\left|\Delta(\partial V/\partial z)\right|$ --- the change in shear that occurs when a thin shear layer flows through a long-wavelength wave --- can be reasonably well predicted using Eq. (10). The inputs needed for this calculation are the long-wave amplitude (a), the mean flow velocity (V_o), the Brunt-Väisälä frequency (N_M), and the long-wave frequency (n).

Figure 19 shows that the occurrence, or lack of occurrence, of wave-induced shear-layer instabilities in the water channel experiments could be predicted fairly consistently using Eq. (13). This equation incorporates Eq. (10) for estimating the wave shear. The criterion for instability that was used is that the shear layer will become unstable when the predicted minimum Richardson number is less than 0.25.

APPLICATION TO ATMOSPHERIC SHEAR FLOWS

In earlier work (Refs. 1 through 4) in this program, clear air turbulence was associated with the destabilization of initially stable shear layers by long gravity waves. Several cases were presented in which the long gravity waves were induced by mountains. Also, a few cases were presented in Ref. 3 in which the long wave-like undulations were induced by thunderstorms. These findings appear to be in agreement with evidence assembled by other investigators --- notably Woods (Ref. 11, a study of wave-induced instabilities in the ocean), Ludlam (Ref. 12, a study of billow cloud formation), Mitchell and Prophet (Ref. 13, an analysis of USAF Project HICAT flight data), Spillane (Ref. 14, an analysis of high-altitude CAT over the Australian desert region), Hardy (Ref. 15, radar measurements that indicated wave-like motions in regions of CAT), Hicks (Ref. 16, radar observations of gravitational waves associated with CAT near the tropopause), Boucher (Ref. 17, radar observations of waves associated with CAT at a subsidence inversion), Gossard, Richter and Atlas (Ref. 18, radar observations of internal gravity waves and billows at an oceanic inversion), Browning and Watkins (Ref. 19, radar observations of billows associated with CAT near a frontal zone beneath the jet core), Browning and Watkins (Ref. 20, radar observations of billows associated with CAT in mountain lee waves), Roach (Ref. 21, aircraft reports of gravity waves associated with CAT over the Atlantic Ocean), Penn and Thompson (Ref. 22, turbulence measurements associated with stable layers which are extensive in area, persist in time and have large vertical wind shears), and Axford (Ref. 23, aircraft observations of gravity waves associated with CAT in the lower stratosphere).

The purpose of the present effort was to develop and evaluate a CAT prediction procedure based on the mechanism of wave-induced instability of initially stable shear layers. The analysis used in the prediction procedure was developed previously during this program and is reviewed in this section. It should be mentioned that some of the wave and turbulence forecasting information used in the development and evaluation of the prediction procedure was provided by United Air Lines and the Air Force Global Weather Central. Also, mountain wave data used to evaluate the UAL wave prediction procedure was obtained from 1968 and 1970 Lee Wave Observational programs at the National Center for Atmospheric Research.

Review of the Fundamental Flow Phenomenon

A schematic diagram of the flow condition considered here is shown in Fig. 20(a). This is analogous to the situation shown in Fig. 13(a) which was used to describe wave-induced shear layer instabilities in the Water Channel. At the left in Fig. 20(a) are shown upstream wind and temperature profiles with a stable shear layer having a thickness 2d. Within this layer, the mean wind is V_o and the mean temperature is T_o; the shear is $(\partial V/\partial z)_o$ and the environmental lapse rate is $\partial T/\partial z$.

At the right in Fig. 20(a) is shown a portion of a long-wavelength wave having an amplitude, a (which might be 2000 or 3000 ft), and a wavelength λ_{LW} (which might be 10 or 20 nmi). It is assumed in this analysis that the thickness of the shear layer, the mean temperature and the lapse rate all remain constant as the flow within the shear layer experiences the undulating motion (2d, T_o, and $\partial T/\partial z$ are constant). The increase in shear that occurs at the crest can be calculated from Eq. (10) given previously. Now, for flows in the atmosphere,

N_M = Brunt-Väisälä frequency = $\sqrt{(g/T_o) \cdot (\partial T/\partial z) - (\partial T/\partial z)_{ad}}$

n = wave frequency = $2\pi V_o/\lambda_{LW}$

$(\partial T/\partial z)_{ad}$ = adiabatic lapse rate, -2.98×10^{-3} deg C/ft*

This increase in shear is added to the initial shear, and Eq. (13) can be used to calculate the minimum Richardson number (which occurs locally at the crest in Fig. 20(a), but would occur at the trough if the initial shear were negative). Since $N_M^2 > n^2$ under most conditions of interest (this is only untrue for weakly stable lapse rates, i.e., when $\partial T/\partial z \approx (\partial T/\partial z)_{ad}$), Eq. (13) can be further simplified to

$$Ri_{MIN} \approx \frac{N_M^2}{\left(\left|(\partial V/\partial z)_o\right| + N_M^2 (a/V_o)\right)^2} \qquad (15)$$

From Eq. (15) it is evident that low values of Ri_{MIN} are associated with large initial shears, $(\partial V/\partial z)_o$; with large long-wave amplitudes, a; and with low winds, V_o. The latter two parameters are not independent, however, since large amplitude waves do not usually occur under low-wind conditions.

The effect of the environmental lapse rate, $\partial T/\partial z$, on Ri_{MIN} is not evident from Eq. (15) but can be seen in Fig. 20(b). This figure is based on typical conditions under which long-wavelength waves, such as mountain lee waves, are observed in the lower stratosphere. Curves are shown for three shears --- small shears (1 and 2 kts/1000 ft) and a moderately large shear (12 kts/1000 ft). The curves show that the greater the initial stability from a convective standpoint (i.e., the greater $\partial T/\partial z$), the lower Ri_{MIN} will be. They also show that shear layers which have small

*Note use of minus sign to denote temperature decreasing with increasing altitude.

values of initial shear are stable when the environmental lapse rate is near zero. Thus, it is primarily the most stable layers appearing in the temperature profile that are of interest. The curves also show that as the environmental lapse rate approaches the adiabatic lapse rate (-3 deg C/ft), all shear layers become unstable.

Previous theoretical and experimental studies which have been discussed in this report have shown that the critical Richardson number below which two-dimensional flows are unstable is 0.25. For $Ri_{MIN} = 0.25$ and fixed values of wave amplitude, a wind velocity, V_o, and wavelength, λ_{LW}, Eq. (13) can be used to determine the neutral stability boundaries on a plot of absolute value of initial wind shear, $\left|(\partial V/\partial z)_o\right|$, versus vertical temperature gradient, $\partial T/\partial z$. The stability boundaries are shown for wave amplitudes of 500 and 3000 ft in Figs. 21 and 22, respectively. The boundaries are shown for wind velocities, V_o, of 10, 25, 50, 75, and 100 kts (λ_{LW} = 15 nmi). Atmospheric flows having combinations of vertical temperature gradient and initial wind shear which plot under the boundary for a given wind velocity would remain stable as they passed through the undulations of the long-wavelength waves. Flows having combinations of $\partial T/\partial z$ and $\left|(\partial V/\partial z)_o\right|$ which plot above the boundary would become unstable. Flows having $\partial T/\partial z < -0.00298$ deg C/ft would be convectively unstable. It is seen in Figs. 21 and 22 that the stability of the flow decreases with decreasing wind velocity.

Figures 21 and 22 could be used with rawinsonde data to predict whether or not initially stable shear layers will be destabilized by long-wavelength waves. For example, V_o, $(\partial V/\partial z)_o$, and $\partial T/\partial z$ would be determined from rawinsonde data and used with Figs. 21 and 22 for weak and strong wave activity, respectively, to make predictions about the stability of the flow. Where flows are predicted to become unstable, CAT could be expected to occur. A more comprehensive approach to CAT prediction is presented in the next section, however.

The variations in maximum allowable initial shear with wind velocity for wave amplitudes of 500, 1000, 2000, and 3000 ft are shown in Fig. 23. For values of initial shear greater than this maximum, the flow for the given wave amplitude would be unstable for all values of vertical temperature gradient. The curves shown in Fig. 23 were obtained using

$$\left|(\partial V/\partial z)_o\right|_{MAX} = \left[1 + (2\pi a/\lambda_{LW})^2\right]\left[V_o/a\right] \qquad (16)$$

Equation (16) was obtained by solving Eq. (13) for $(\partial V/\partial z)_o$, differentiating with respect to the Brunt-Väisälä frequency, and solving for the maximum value of $\left|(\partial V/\partial z)_o\right|$. For long wavelengths, i.e., $\lambda_{LW} > 2\pi a$, Eq. (16) can be simplified to

$$\left|(\partial V/\partial z)_o\right|_{MAX} = V_o/a \qquad (17)$$

The variation of $\left|(\partial V/\partial z)_o\right|_{MAX}$ with V_o for a = 3000 ft was determined using Eq. (17) and is compared in Fig. 23 (dashed curve) with that obtained using Eq. (16). For $\lambda_{LW} \geq 15$ nmi and a = 3000 ft, the difference in values of $\left|(\partial V/\partial z)_o\right|_{MAX}$ is quite small. This difference would be even less for smaller wave amplitudes.

Improved CAT Prediction Methods

In general, most CAT prediction techniques are based on synoptic features which are present and on a comparison of the values of one or more atmospheric parameters (such as horizontal wind shear, vertical wind shear, horizontal temperature gradient, streamline curvature, etc.) with empirically determined critical values. In most cases, there is no physical model for the breakdown mechanism. An example of such a prediction technique is given in Ref. 24. The technique is based on horizontal and vertical temperature gradients (determined from rawinsondes along the flight route) and is quite simple to use.

In Ref. 3 it was recommended that consideration be given to development of a prediction procedure which would predict the altitudes where CAT would be encountered in mountain waves and which is based on the mechanism of wave-induced instability of initially stable shear layers. During the present program, such a procedure was developed and evaluated. Evaluation was limited, however, because of the limited amount of available data. This procedure was comprised of three distinct operations contained in a single computer program which is discussed in detail in Ref. 5: (1) the rawinsonde data from a given station is processed to predict the long-wave amplitude necessary to destabilize each shear layer appearing in the profiles; (2) meteorological data from mountain wave zones are used with wave prediction methods to predict lee wave activity and amplitudes; and (3) the results from (1) and (2) are compared to see if wave-induced instabilities would occur and to identify the associated altitudes and locations. A block diagram of the computer program logic is shown in Fig. 24.

Calculation of Required Long-Wave Amplitudes

This portion of the procedure is relatively straight-forward. Equation (13) can be rewritten to yield the minimum long-wave amplitude necessary to destabilize (Ri_{MIN} = 0.25) a shear layer:

$$a = \frac{2N_M - |(\partial V/\partial z)_o|}{N_M^2 - n^2} \cdot V_o \qquad (18)$$

The rawinsonde data are processed by the computer program to identify stable shear layers (using temperature and velocity profiles) and, for each layer, to calculate the mean flow parameters V_o, $(\partial V/\partial z)_o$, N_M, and n. In calculating $n = 2\pi V_o/\lambda_{LW}$, it is necessary to assume a value for the wavelength, λ_{LW}. In general, λ_{LW} is of the order of 15 nmi and (for atmospheric flows) n is small compared to N_M so that large errors in n have little effect on the computed amplitude, a. Using the mean flow parameters and an assumed long-wave wavelength, the required amplitude for instability is calculated for stable shear layers which have temperature gradients greater than some preselected minimum value (for a given wave amplitude, the induced wave shear, $\Delta(\partial V/\partial z)$, increases with increasing stability so that the most stable layers are the most likely to experience instabilities).

Long-Wave Amplitude Forecast

At this point, the characteristics of waves in the local zone of the forecast must be considered. To forecast CAT induced by mountain lee waves, good techniques for forecasting the occurrence and amplitudes of lee waves are required. The techniques which are used by those active in forecasting mountain wave CAT, such as United Air Lines (Ref. 25), Northwest Airlines, and Global Weather Central at Offutt Air Force Base, are empirical and rely on such parameters as wind direction and strength above the mountains, sea level pressure difference across the mountains, lapse rate and synoptic conditions in the local zone of forecast. When significant wave activity is forecast, attempts are made to avoid flying within approximately $\pm$5000 ft of the tropopause.

United Air Lines uses synoptic data in the forecast zone to forecast the occurrence of mountain waves and CAT. During the forecast period, they check their forecast with a nomogram which uses sea level pressure difference across the mountains and maximum wind velocity between 10,000 and 20,000 ft (perpendicular to the mountains) to predict mountain wave activity for 20 wave zones in the United States. This nomogram, which is shown in Fig. 25, was first used to predict the Denver wave. The pressure difference used was the sea level pressure at Grand Junction minus the sea level pressure at Denver. In using the nomogram for other wave zones, where the distance between the stations may be different than the distance between Grand Junction and Denver, a pressure correction is required. The magnitude of the correction depends on the difference in distance, and the correction is plus if the distance is less and minus if the distance is greater. The wave zones and pressure corrections are given in Ref. 25. Pressure tendency is often used to extend the period of validity of the nomogram.

The nomogram (Fig. 25) indicates no lee waves would be expected when the maximum wind velocity perpendicular to the mountain was less than 20 kts. For maximum wind velocities above 20 kts, the strength of the wave depends on the sea level pressure difference. Northwest Airlines also uses the nomogram shown in Fig. 25 to predict the presence of mountain waves; however, they use the wind velocity perpendicular to the mountains at 300 mb altitude rather than maximum wind velocity between 10,000 and 20,000 ft. Global Weather Central has correlated the coordinates on the nomogram with the severity of turbulence and uses the pressure difference and maximum winds (between 10,000 and 20,000 ft, perpendicular to the mountains) to predict the occurrence and severity of CAT.

Some data obtained by the author during the 1970 Lee Wave Observation Program at the National Center for Atmospheric Research for the Grand Junction-Denver wave zone are plotted on Fig. 25 for comparison with the nomogram. The data obtained about 0500 MST between February 11 and February 27. The numbers next to the data points denote the date. Flights were made on February 13, 17, 18, and 26 to make measurements in the wave field (flights were only made on days when wave activity was forecast by other techniques). Results of these flights indicated that weak waves were present on February 13 and 26, and weak to moderate or strong waves were present on February 17 and 18. Isentropes reconstructed from flight and radiosonde data which show the mountain wave patterns which occurred on February 13, 17, and 18 are shown in Figs. 19, 21, and 23 of Ref. 3. The data points which correspond to days on which flights were made are flagged (a weak wave observation is indicated by a single flag and a moderate wave by a double flag).

The data for which wave activity was confirmed by flights is in fairly good agreement with the nomogram. For instance, the nomogram indicates (1) the presence of weak waves on February 12, 13, and 14 --- weak waves were observed on February 13, and (2) the presence of weak waves on February 16 and 18 and moderate to strong waves on February 17 --- moderate waves were observed on February 17 and 18. Wave amplitudes up to 1000, 1350, and 1800 ft were observed on February 13, 17, and 18, respectively. Also, on days for which flights were not made (because no wave activity was forecast by other more complicated techniques), most of the data (February 15, 19, 21, 22, 23, and 24) fall into the "no wave" region of the nomogram. Although negative pressure differences were not considered in Ref. 25, it is felt that waves would not occur under such conditions.

It appears then that if such a nomogram could be modified to provide wave amplitude information it could be used with rawinsonde data to predict the altitude where CAT would occur from destabilization of initially stable layers by mountain waves. Pressure tendency and forecast winds might be used with the nomogram to forecast the occurrence of mountain lee waves and the altitude where CAT would occur from destabilization of stable shear layers by the lee waves.

This nomogram was used, in modified form, to provide wave amplitude information and was incorporated in the computer program for predicting mountain-wave induced shear-layer instability resulting in CAT. A correlation of wave amplitude with nomogram-predicted wave activity was attempted by the present author using observed wave amplitudes for the three mountain wave patterns for February 13, 17, and 18 (presented in Ref. 3) with predicted wave activity for those days. Nomogram-predicted wave activity and wave amplitude are compared in Sketch F. In lee wave patterns presented previously in Ref. 1, wave amplitudes up to 3000 and 3500 ft are apparent. Although nomogram-predicted wave activity is not available for these cases, the data were plotted in Sketch F in the region of moderate or strong wave activity.

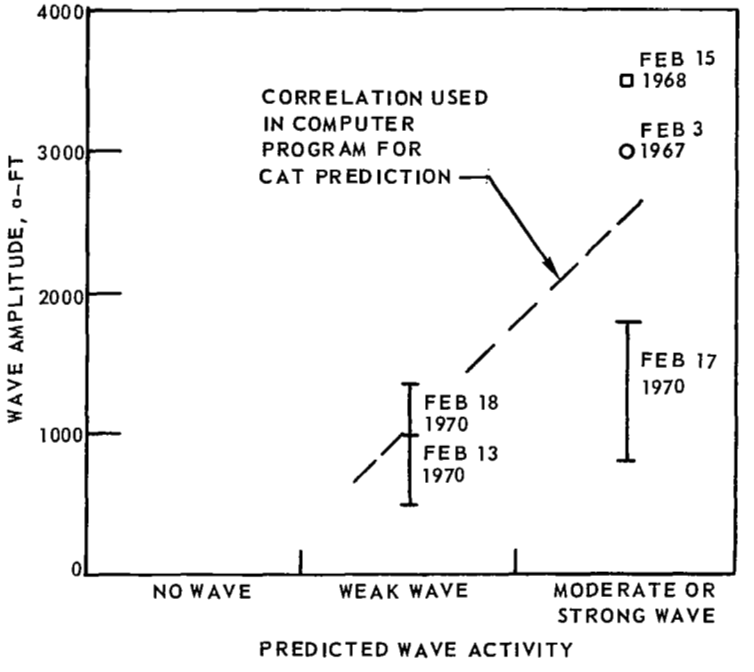

SKETCH F. CORRELATION OF WAVE AMPLITUDE WITH PREDICTED WAVE ACTIVITY

Based on the data presented in Sketch F, wave amplitudes of 1000 and 2500 ft were selected to correlate weak and moderate or strong wave activity, respectively. Because of the scarcity of data, the accuracy of this correlation is admittedly questionable. Also, since amplitudes of 1000 and 2500 ft are less than the maximum amplitudes observed for the corresponding wave activities, CAT may be underpredicted by the computer program (use of amplitudes equal to 1400 and 4000 ft for weak and moderate or strong wave activities, respectively, would probably be more conservative). However, the selected correlation between wave amplitude and activity could be changed based on experience and new data.

The computer program (Fig. 24) then, predicts lee wave amplitudes of 1000 and 2500 ft when weak and moderate or strong wave activity is predicted, respectively. This provides a means for estimating lee wave amplitude from sea level pressure difference and maximum wind velocity perpendicular to the mountains in the altitude range from 10,000 to 20,000 ft.

Screening and CAT Forecast

At this point, the computer program (Fig. 24) compares the wave amplitudes required to destabilize each initially stable layer with the predicted amplitude of the mountain lee wave. Layers requiring amplitudes smaller than the lee wave amplitude would be expected to become unstable and produce CAT. Then, when weak waves (a = 1000 ft) were forecast, turbulence would be forecast within $\pm$1000 ft of the altitude of layers which were predicted to become unstable and when strong waves (a = 2500 ft) were forecast, turbulence would be forecast within $\pm$2500 ft of the altitude of unstable layers.

Computer Program for Forecasting Mountain Lee Wave CAT

Referring to Fig. 24, the program first computes the vertical velocity and temperature profiles and the velocity and temperature gradients for each layer from rawinsonde data obtained upwind from the mountains (block (1)). The program then identifies stable shear layers from the velocity and temperature profile data and selects those which are of interest for further analysis (temperature gradient above preselected minimum value). Next, the program calculates the lee wave amplitude required to destabilize (reduce Ri_{MIN} to 0.25) these stable shear layers, using from the rawinsonde data the initial shear, $(\partial V/\partial z)_o$, velocity, V_o, temperature gradient, $(\partial T/\partial z)_o$, and temperature, T_o (block (2)).

In the next step (block (3)), the program uses the United Air Lines nomogram (with the amplitude modification made by the author) to (a) predict lee wave activity and amplitudes using values of pressure difference and maximum wind velocity or (b) forecast future lee wave activity and amplitudes using pressure tendency and forecast wind velocity. The program then (block (4)) compares the predicted amplitude of the lee waves with the amplitudes required to destabilize the stable shear layers. CAT is predicted to occur at altitudes corresponding to layers which are predicted to become unstable.

Concluding Remarks

Previous analyses of CAT cases involving mountain waves (Refs. 1 and 3) have shown that there is a fair to good agreement between the altitudes at which CAT was detected and the altitudes of initially stable layers which were predicted to be destabilized by the wave-induced shear. Measured lee wave amplitude was used in these analyses and in general the amplitude varied with altitude. The UAL nomogram, which is based on airline experience, does quite well in predicting current wave activity using current pressure difference and maximum wind velocity. Data obtained in the 1970 Lee Wave Observation program tend to confirm this. Also, based on lee wave observations, it does not appear unreasonable to correlate wave amplitude with wave activity. However, using the nomogram there is no way of estimating the variation in wave amplitude with altitude. The success in using the nomogram with the computer program to forecast future wave activity will depend on the success in using pressure tendency to forecast pressure difference and success in forecasting the maximum wind velocity. The forecast might be quite good for short forecast periods. The major advantage in using the nomogram is that it is quite simple to use with the computer program. However, if the nomogram results in erroneous wave forecasts or long range forecasts are desired, then more subjective techniques could be used for forecasting lee wave activity as suggested in the lower part of Fig. 24. Such techniques are presently in use by UAL, USAF, and others and use synoptic data, such as the change in height of the tropopause upwind from the mountains, wind velocity in the wave zone, wind and isotherm patterns, and location of warm tongues of air at 850 mb to the lee of the mountains to forecast mountain waves. It does not appear that a technique such as this could be included in the computer program; if such a technique were used, some way of estimating the wave amplitude is again required.

REFERENCES

1. Clark, J. W., R. C. Stoeffler, and P. G. Vogt: Research on Instabilities in Atmospheric Flow Systems Associated with Clear Air Turbulence. NASA Contractor Report CR-1604, prepared under Contract NASW-1582, June 1970; also United Aircraft Research Laboratories Report H910563-9, June 1969.

2. Clark, J. W.: Laboratory Investigations of Atmospheric Shear Flows Using an Open Water Channel. Paper presented at AGARD-NATO Specialists' Meeting on "The Aerodynamics of Atmospheric Shear Flows", Munich, Germany, September 15-17, 1969. AGARD Conference Proceedings No. 48, February 1970.

3. Stoeffler, R. C.: Further Research on Instabilities in Atmospheric Flow Systems Associated with Clear Air Turbulence. United Aircraft Research Laboratories Report J910563-14, prepared under Contract NASW-1582, June 1970.

4. Stoeffler, R. C. and J. W. Clark: Research on Instabilities in Atmospheric Flow Systems Associated with Clear Air Turbulence. Abstracts of NASA Contractors Meeting on Aeronautical Fluid Mechanics, June 15-17, 1971, Washington, D. C.

5. Stoeffler, R. C.: Additional Research on Instabilities in Atmospheric Flow Systems Associated with Clear Air Turbulence. United Aircraft Research Laboratories Report K910563-19, prepared under Contract NASW-1582, August 1971.

6. Drazin, P. G.: The Stability of a Shear Layer in an Unbounded Heterogeneous Inviscid Fluid. Journal of Fluid Mechanics, Vol. 4, 1958, pp. 214-224.

7. Hazel, P.: Instabilities of Stratified Shear Flow. Paper submitted for publication in Journal of Fluid Mechanics, 1968.

8. Chandrasekhar, S.: Hydrodynamic and Hydromagnetic Stability. Oxford University Press, London, 1961, p. 491.

9. Phillips, O. M.: The Dynamics of the Upper Ocean. Cambridge University Press, 1966.

10. Haurwitz, B.: Dynamic Meteorology. McGraw-Hill Book Company, Inc., New York, 1941.

11. Woods, J. D.: Wave-Induced Shear Instability in the Summer Thermocline. Journal of Fluid Mechanics, Vol. 32, 1968, pp. 791-800.

REFERENCES (Continued)

12. Ludlam, F. H.: Characteristics of Billow Clouds and Their Relation to Clear Air Turbulence. Quarterly Journal of the Royal Meteorological Scoeity, Vol. 93, 1967, pp. 419-435.

13. Mitchell, F. A. and D. T. Prophet: Meteorological Analysis of Clear Air Turbulence and Its Detection. Boeing Scientific Research Laboratories Report D1-82-0740, Seattle, Washington, August 1968.

14. Spillane, K. T.: Clear Air Turbulence and Supersonic Transport. Nature, Vol. 214, No. 5085, April 15, 1967, pp. 237-239.

15. Hardy, K. R.: Radar Echoes from the Clear Air. Paper prepared for NATO Advanced Study Institute on the Structure of the Lower Atmosphere and Electromagnetic Wave Propagation, Aberystwyth, Wales, September 2-15, 1967.

16. Hicks, J. J.: Radar Observations of a Gravitational Wave in Clear Air Near the Tropopause Associated with CAT. Journal of Applied Meteorology, Vol. 8, August 1969, pp. 627-633.

17. Boucher, R. J.: CAT at a Subsidence Inversion: A Case Study. Journal of Applied Meteorology, Vol. 9, June 1970, pp. 534-537.

18. Gossard, E. E., J. H. Richter, and D. Atlas: Internal Waves in the Atmosphere from High-Resolution Radar Measurements. Journal of Geophysical Research, Vol. 75, No. 18, June 20, 1970, pp. 3523-3536.

19. Browning, K. A. and C. D. Watkins: Observations of Clear Air Turbulence by High Power Radar. Nature, Vol. 227, July 18, 1970, pp. 260-263.

20. Browning, K. A., et al.: Simultaneous Measurements of CAT by Aircraft and Radar. Nature, Vol. 228, December 12, 1970.

21. Roach, W. T.: Some Aircraft Reports of High-Level Turbulence. The Meteorological Magazine, Vol. 98, No. 1160, March 1969, pp. 65-78.

22. Penn, S. and G. J. Thompson: Stable Laminae Associated with Clear Air Turbulence. Paper Presented at Royal Aeronautical Society International Conference on "Atmospheric Turbulence", London, May 18-21, 1971.

REFERENCES (Concluded)

23. Axford, D. N.: An Observation of Gravity Waves in Shear Flow in the Lower Stratosphere. Quarterly Journal of the Royal Meteorological Society, Vol. 96, 1970, pp. 273-286.

24. Ashburn, E. V., D. E. Waco, and F. A. Mitchell: Development of High Altitude Clear Air Turbulence Models. Air Force Flight Dynamics Laboratory Report AFFDL-TR-69-79, prepared by Lockheed California Company, November 1969.

25. Harrison, H. T. and D. F. Sowa: Mountain Wave Exposure on Jet Routes of Northwest Airlines and United Air Lines. UAL Meteorology Circular No. 60, February 1, 1966.

26. Atlas, D. and J. I. Metcalf: The Amplitude and Energy of Breaking Kelvin-Helmholtz Waves and Turbulence. The University of Chicago (Department of Geophysical Sciences) and Illinois Institute of Technology (Department of Electrical Engineering) Laboratory for Atmospheric Probing, Technical Report No. 19, October 26, 1970.

27. Thorpe, S. A.: Kelvin-Helmholtz Instability and Turbulence. Paper Presented at Royal Aeronautical Society International Conference on "Atmospheric Turbulence", London, May 18-21, 1971.

LIST OF SYMBOLS

a	Amplitude of wave (half the height from trough to peak), ft or in.
a_c	Critical lee wave amplitude required to destabilize shear layer in atmosphere, ft
b	Exponent in theoretical velocity profile (Eq. (6)), dimensionless
c	Complex wave velocity, $c = c_r + i \cdot c_i$, ft/sec
c_i	Imaginary part of complex wave velocity, ft/sec
c_r	Real part of complex wave velocity, ft/sec
d	Shear-layer scale length parameter for describing velocity profiles, $d = (\Delta V/2)/(\partial V/\partial z)_o$, ft
E	Kinetic energy per unit volume associated with shear (Eq. (27)), ft-lb/ft^3
g	Gravitational constant, 32.2 ft/sec^2
i	Unit imaginary number, $\sqrt{-1}$, dimensionless
n	Wave frequency, $2\pi V_o/\lambda_{LW}$, sec^{-1}
N_M	Brunt-Väisälä frequency, $N_M = \sqrt{(g/T_o)\cdot\left[(\partial T/\partial z)-(\partial T/\partial z)\right]_{ad}}$ in the atmosphere and $\sqrt{(-g/\rho)(\partial\rho/\partial z)}$ in the Water Channel, sec^{-1}
Ri	Richardson number, $Ri = (g/T_o)\cdot\left[(\partial T/\partial z)-(\partial T/\partial z)_{ad}\right]/(\partial V/\partial z)^2$ in the atmosphere and $(-g/\rho)\cdot(\partial\rho/\partial z)/(\partial V/\partial z)^2$ in the Water Channel, dimensionless
Ri_o	Initial or upstream Richardson number, dimensionless
Ri_{MIN}	Minimum Richardson number caused by influence of long-wavelength wave, dimensionless
t	Time, sec
T	Temperature, deg C, K, or F
T_o	Temperature at center of shear layer, deg C, K, or F

LIST OF SYMBOLS (Continued)

V	Velocity or maximum velocity perpendicular to mountains between 10,000 and 20,000 ft, ft/sec or kts
V_o	Velocity at center of shear layer or velocity of long-wavelength wave, ft/sec or kts
V_1, V_2	Velocities in upper and lower streams bounding shear layer, respectively, for hyperbolic tangent profiles, ft/sec
$w(x,z,t)$	Perturbation velocity (Eq. (9)), ft/sec
w	Width of "Three-Dimensional" **shear layer** (Fig. 6), $w = w_s + 2w_t$, in.
w_s	Width of part of "Three-Dimensional" shear layer containing no horizontal transverse velocity gradient (Fig. 6), in.
w_t	Width of "Three-Dimensional" transition region where shear profile changes to uniform profile (Fig. 6), in.
W_B	Buoyant work per unit volume (Eq. (26)), ft-lb/ft^3
W_F	Kinetic energy per unit volume associated with lateral motion (Eq. (32)), ft-lb/ft^3
W_T	Total work per unit volume (Eq. (33)), ft-lb/ft^3
x	Downstream coordinates in Water Channel (Fig. 1), ft or in.
y	Transverse coordinate in Water Channel (Fig. 1), ft or in.
z	Vertical coordinate in Water Channel (Fig. 1), ft or in.
z_o	Vertical coordinate of center of shear layer in Water Channel, or mean altitude of stable layer in the atmosphere, ft or in.
z_1, z_2	Vertical distance to V_1 and V_2, respectively, in.
α	Wavenumber of small-amplitude waves associated with instabilities in shear layers, $\alpha = 2\pi/\lambda$, ft^{-1}

LIST OF SYMBOLS (Concluded)

β	Parameter in density profile equation (Eq. (2)), $\beta = Ri \cdot d \cdot (\partial V/\partial z)_o^2/g$, dimensionless
Δp	Sea level pressure difference, (Fig. 25), mb
ΔV	Velocity difference parameter for describing velocity profiles (Eq. (1)), ft/sec
δ	Increment in quantity, dimensionless
$\Delta(\partial V/\partial z)$	Change in shear caused by influence of long-wavelength wave, sec^{-1}
$(\partial T/\partial z)_{ad}$	Adiabatic lapse rate, $(\partial T/\partial z)_{ad} = -2.98 \times 10^{-3}$ deg C/ft
$(\partial T/\partial z)_o$	Initial upstream temperature gradient, deg F/ft or deg C/1000 ft
$(\partial V/\partial z)_o$	Initial or upstream shear, sec^{-1} or kts/1000 ft
$(2d)_m$	Measured thickness of shear layer before turbulent breakdown, in.
λ	Wavelength of small-amplitude waves associated with instabilities in shear layers, ft or in.
λ_{LW}	Wavelength of lee wave or long-wavelength wave in Water Channel, in., ft, or nmi
ν	Kinematic viscosity, ft^2/sec
ρ	Density of water or air, $slugs/ft^3$
ρ_o	Denisty of water or air at center of shear layer, $slugs/ft^3$
ρ_1, ρ_2	Densities in upper and lower streams bounding shear layer, respectively, $slugs/ft^3$
$\phi(z)$	Perturbation amplitude function in shear-layer stability analysis, ft^2/sec
ψ'	Perturbation stream function in shear-layer stability analysis, ft^2/sec

APPENDIX I: METHOD FOR FITTING HAZEL'S THEORETICAL VELOCITY PROFILE TO DATA FOR "S-SHAPED" VELOCITY PROFILES

This Appendix describes the method which was used to fit the theoretical velocity profile of Hazel (Ref. 7) to the "S-shaped" velocity profiles obtained experimentally in the UARL Open Water Channel. The theoretical profile was given previously in Eq. (6). It will also be helpful to refer back to Sketch C in the main text.

Fitting Eq. (6) to a measured profile involves determining the constants b, ΔV, and d. In the following development this will be done by matching the velocities V_1 and V_2 at z_1 and z_2, the shears at z_1 and z_2 (which are zero), and the mean shear, $(\partial V/\partial z)_o$, at z_o of the measured profile to those of the theoretical profile.

The shear can be obtained by differentiating Eq. (6) with respect to the vertical coordinate z:

$$\partial V/\partial z = \left(\frac{\partial V}{\partial z}\right)_o \left\{\left[(b+1)\ \mathrm{sech}^2\left(\frac{z-z_o}{d}\right)\right] - b\right\} \mathrm{sech}^b\left(\frac{z-z_o}{d}\right) \tag{19}$$

In this equation, the following substitution was made:

$$(\partial V/\partial z)_o = \frac{\Delta V}{2d} \tag{20}$$

At z_1 the shear is zero, so Eq. (19) yields

$$\mathrm{sech}\left((z_1-z_o)/d\right) = \sqrt{\frac{b}{b+1}} \tag{21}$$

Substitution of Eq. (21) into Eq. (6) provides an expression for V_1:

$$V_1 = V_o + \left(\frac{\Delta V}{2}\right) b^{\frac{b}{2}} (b+1)^{-\frac{b+1}{2}} \tag{22}$$

Replacement of V_o with $(V_1 + V_2)/2$ in Eq. (22) yields an equation for ΔV as a function of b, V_1, and V_2:

$$\Delta V = (V_1 - V_2)\ b^{-\frac{b}{2}} (b+1)^{\frac{b+1}{2}} \tag{23}$$

Now, substitution of ΔV from Eq. (20), $(z_1 - z_o)/d$ from Eq. (21) and $V_o = (V_1 + V_2)/2$ into Eq. (22) results in

$$\left[(z_1 - z_o)/(V_1 - V_2)\right](\partial V/\partial z)_o = \frac{1}{2}\left(\mathrm{arccosh}\left(\frac{b+1}{b}\right)^{\frac{1}{2}}\right) b^{-\frac{b}{2}} (b+1)^{\frac{b+1}{2}} \tag{24}$$

Using a similar development but with the condition that the shear is also zero at z_2 yields an expression that is similar to Eq. (24) except that z_1 is replaced by z_2 and the right side of the equation is negative. Combining this result with Eq. (24) produces

$$\left[(z_1 - z_2)/(V_1 - V_2)\right](\partial V/\partial z)_0 = \left(\operatorname{arccosh}\left(\frac{b+1}{b}\right)^{\frac{1}{2}}\right) b^{-\frac{b}{2}} (b+1)^{\frac{b+1}{2}} \tag{25}$$

The left side of Eq. (25) can be determined entirely from properties of the measured profile. The right side is only a function of b. Therefore, the value of b for a given profile can be obtained by plotting b versus the right side of Eq. (25) and entering the plot at the value given by the left side of Eq. (25). After obtaining b for the profile, ΔV can be obtained from Eq. (23) and, finally, d can be obtained from Eq. (20). Thus, all of the parameters needed in Eq. (6) to describe the velocity V as a function of z have been determined.

APPENDIX II: SUMMARY OF OTHER FLUID MECHANICS INVESTIGATIONS

Experimental Investigations of Stability of Straight, Stratified, Shear Flows Having Multiple Shear Layers

The purpose of these investigations was to investigate the stability of a shear layer consisting of a combination of several thinner stable and unstable layers. Experiments were conducted to investigate conditions under which such flows become unstable and the characteristics of the flow during the initial phases of breakdown.

Description of Combined Shear Layer Experiments

The two types of velocity profiles which were investigated are shown in Sketch G. The profiles are designated Type LSL and Type SLS (S for small shear and L for large shear). Type LSL velocity profile consists of a layer having small shear sandwiched

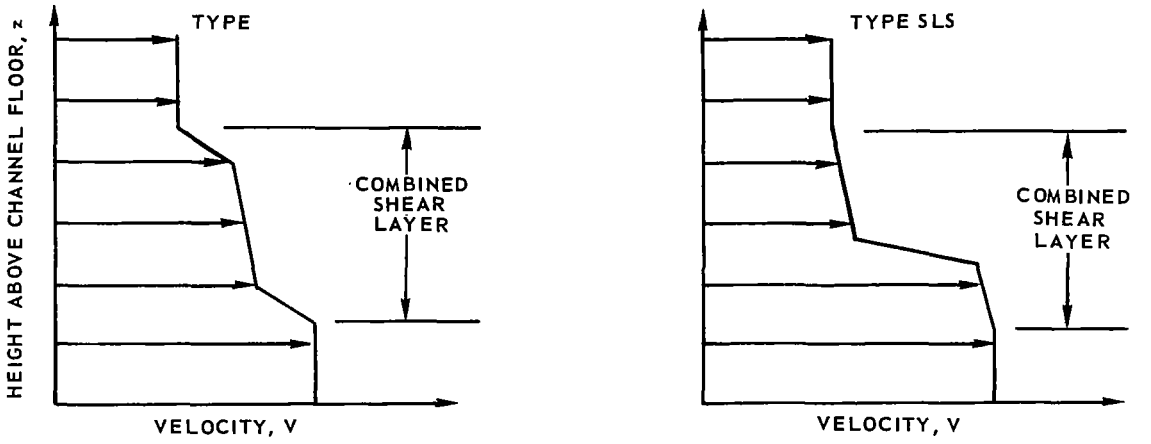

SKETCH G. VELOCITY PROFILES USED IN STABILITY TESTS OF COMBINED SHEAR LAYERS

between two layers having large shears. Type SLS consists of a layer having large shear sandwiched between two layers having small shears. Tests were made to determine if turbulent breakdown of layers having large shears would cause a combined shear layer, consisting of unstable large-shear layers and stable small-shear layers, to become unstable and break down. Accordingly, attempts were made to establish density gradients which would stabilize the small-shear layers ($Ri > 0.25$) but not the large-shear layers ($Ri < 0.25$).

Summary of Experimental Results

Typical velocity, temperature, and density profiles for the combined shear layer experiments are shown in Fig. 26. Profiles for a type LSL combined layer having a layer of small shear ($\partial V/\partial z$ = -0.26 sec^{-1}) sandwiched between two layers of large shear (lower layer $\partial V/\partial z$ = -2.7 sec^{-1} --- upper layer $\partial V/\partial z$ = -0.65 sec^{-1}) are shown in Fig. 26(a). The Richardson numbers, Ri, for the upper, middle, and lower shear layers were 0.044, 0.272, and 0.003, respectively. Thus, the upper and lower layers would be expected to become unstable and the middle layer to be marginally stable.

The stages of breakdown which were observed during this test are sketched in Fig. 27(a). First, there is a region where the flow appears to be undisturbed. Then waves appear in the unstable layers. The waves in the upper layer (V_o equal to 0.02 ft/sec) have a wavelength, λ, of 4 in. and appear upstream from the waves in the lower layer (V_o equal to 0.09 ft/sec) which have a wavelength of 2 in. The waves grow in amplitude and then transition to vortices. Further downstream the vortices interact with each other causing turbulent breakdown of the combined layer. In the turbulent region there was some evidence that the combined layer was influencing the breakdown. There appeared to be an overall swirling motion superimposed on the turbulence. This swirling motion was periodic and had a wavelength, λ, approximately equal to 8 in. This wavelength is more characteristic of the length expected based on the combined layer thickness than on the thickness based on any of the individual layers and suggests, therefore, that the combined layer is influencing the breakdown (from Refs. 1 and 3, the expected wavelength is $(\sqrt{2\pi})\cdot 2d$).

Typical profiles for combined layer type SLS having a layer of large shear sandwiched between two layers of small shear are shown in Fig. 26(b). The Richardson numbers, Ri, for the upper, middle, and lower shear layers were 2.02, 0.014, and 0.21, respectively. Thus, the upper layer would be expected to be stable, the lower layer to be slightly unstable, and the middle layer unstable. The stages of breakdown which were observed during this test are sketched in Fig. 27(b). First, there is a region where the flow appears undisturbed. Then waves appear which have a wavelength, λ, equal to 4 in. These waves grow in amplitude and then transition to vortices. Further downstream some of these vortices continue to grow in size and some are suppressed. The wavelength associated with the growing vortices was 8 in. and, based on the thickness of the layers, was more characteristic of the combined layer than any of the individual layers. Further downstream, turbulent breakdown occurred as the growing vortices interacted with each other and the suppressed vortices.

Observations of the stages of breakdown during these tests indicated that the breakdown of the unstable layers was not independent of the adjacent stable layers. The growth of instabilities initiated in the unstable layers appeared to be fed in part by the shear energy from the adjacent stable shear layers. The final stages of

the breakdown appeared to be influenced by the combined layer at its characteristic wavelength. This was most obvious in the test of combined layer type SLS. Here, then, is a case where small amplitude instabilities having short wavelengths result in larger amplitude instabilities having longer wavelengths.

These results are in agreement with theoretical work done by Atlas (Ref. 26) and experimental results obtained by Thorpe (Ref. 27). Atlas showed that once the minimum Richardson number in a layer decreases to a value less than 0.25, any resulting instability would grow in amplitude until the layer Richardson number was 0.5 (losses because of dissipation would result in growth to a layer Ri less than 0.5). Thus, a thin, unstable ($Ri < 0.25$) shear layer in a thick slightly stable ($Ri > 0.25$) shear layer may result in the destabilization of the thick as well as the thin layer, provided the layer Richardson number is 0.5. The layer Richardson number is an average Richardson number based on the initial velocity and density profiles and a layer thickness equal to twice the maximum amplitude of the instability. Thorpe has observed that when the Kelvin-Helmholtz type of instability occurs in stratified shear flows the volume of turbulent fluid grows until the layer Richardson number is about 0.4.

Concluding Remarks

The results of these experiments indicate that, for the type of velocity and temperature profiles tested, the breakdown of combined shear layers consisting of stable and unstable layers is initiated by the instability of the unstable layers and that the final stages of breakdown are influenced by the combined layer at its characteristic wavelength. The observations indicated that, in combined shear layers, the small amplitude short-wavelength disturbances associated with the initial instability can result in large amplitude, long-wavelength disturbances.

Stability Criterion for "Three-Dimensional", Straight, Stratified Shear Flows

The value of stability criteria derived by energy methods is open to question. However, since such criteria have been derived by other investigators, a simple criterion for the three-dimensional case was derived and is presented in this Appendix. Chandrasekhar (Ref. 8) determined the critical value of Richardson number for two-dimensional stratified shear flows using energy considerations. Chandrasekhar reasoned that for a stably stratified shear flow to become unstable there must be enough kinetic energy available from the shear to work against the buoyant stabilizing forces. Chandrasekhar determined the critical Richardson number by equating the work required to interchange fluid particles (1) and (2), shown in Sketch H, to the kinetic energy available from the difference in velocity between particles (1) and (2).

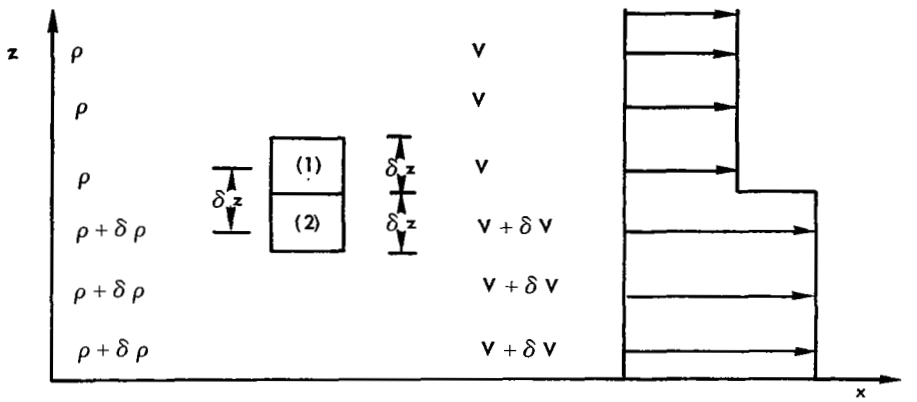

SKETCH H. DENSITY AND VELOCITY DISTRIBUTION FOR TWO-DIMENSIONAL STABLY STRATIFIED SHEAR FLOW ANALYSED BY CHANDRASEKHAR

It was shown (Ref. 8) that the work per unit volume, W_B, required to interchange particles (1) and (2) is given by

$$W_B = -g \cdot \delta\rho \cdot \delta z \tag{26}$$

and that the kinetic energy per unit volume, E, available from the shear layer is given by

$$E = \rho(\delta V)^2/4 \tag{27}$$

For instability to occur, E must be greater than W_B:

$$W_B/E = -\frac{g \cdot \delta\rho \cdot \delta z}{\rho(\delta V)^2/4} < 1.0 \tag{28}$$

The critical Richardson number is obtained by dividing the numerator and denominator in Eq. (28) by δz and is given by

$$-\frac{g(\delta\rho/\delta z)}{\rho(\delta V/\delta z)^2} = Ri < 0.25 \tag{29}$$

Thus, for two-dimensional stably stratified shear flows one would expect instability to occur when the Richardson number was less than 0.25. This result is in agreement with theoretical stability criteria of Drazin, Hazel, and others. It is also in agreement with experimental results obtained in this program and reported previously in Refs. 1 through 5.

The method of Chandrasekhar was extended to investigate the stability of "three-dimensional" stably stratified shear flows for which the thickness of the shear layer was small compared to the width of the shear layer; i.e., the velocity profile was three-dimensional. A side view of the flow sectioned through the shear layer on the centerline of the "three-dimensional" flow is the same as that shown in Sketch H. A front view of the flow after fluid particles (1) and (2) have been interchanged is shown in Sketch I.

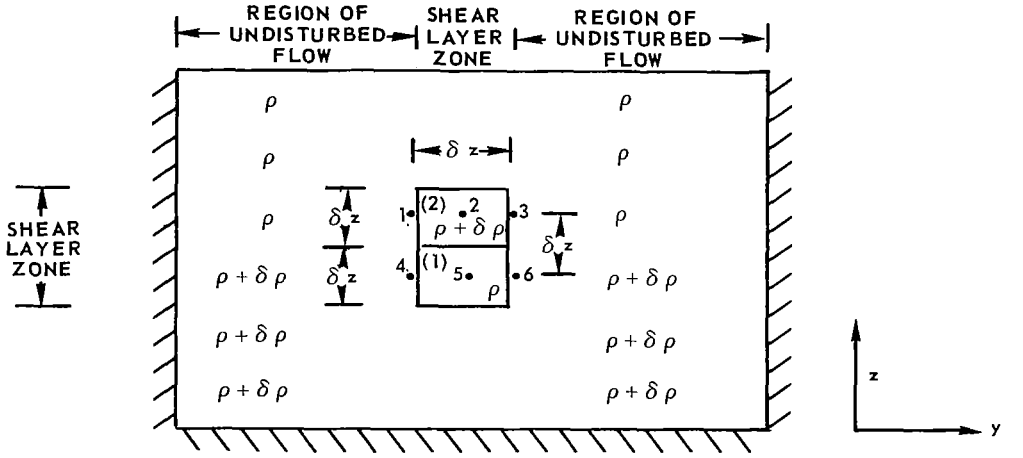

SKETCH I. FRONT VIEW OF "THREE-DIMENSIONAL" STABLY STRATIFIED SHEAR FLOW ANALYSED USING METHOD OF CHANDRASEKHAR

In Sketch I, the flow direction is out of the paper. For this analysis it is assumed that horizontal velocity gradients are negligible. The difference in velocity and density between particles (1) and (2) is δV and $\delta\rho$, respectively.

The critical Richardson number of the three-dimensional flow shown in Sketch I can be obtained, in a manner similar to the method used for two-dimensional flows, by equating the kinetic energy per unit volume available from the shear to the energy per unit volume required to interchange particles (1) and (2). The work per unit volume, W_B, required to overcome buoyant forces and the kinetic energy per unit volume, E, available from the shear are the same for the three-dimensional flow as for the two-dimensional flow and were given previously in Eqs. (26) and (27), respectively. However, for the three-dimensional flow, as particles (1) and (2) are interchanged, pressure forces occur which tend to make the fluid spread laterally. This lateral motion does not help destabilize the flow and, since the kinetic energy per unit volume of this motion must also come from the kinetic energy per unit volume associated with the shear, the three-dimensional flow appears more stable than the two-dimensional

flow. The kinetic energy per unit volume associated with the lateral motion was assumed to be equal to the potential energy per unit volume associated with the lateral pressure forces which would act on the particles if the particles were restrained from moving laterally while they are being interchanged. The lateral pressure forces, which are equal to potential energy per unit volume, result from the differences between the pressure at the center of particles (1) and (2) (at points 2 and 5 shown in Sketch I) and the pressure at the sides (at points 1, 3, 4, and 6) of the particles. These pressure differences, which are equivalent to potential energy per unit volume, are given by

$$(P_2 - P_1)_{(2)} = (P_2 - P_3)_{(2)} = g \cdot \delta\rho \cdot \delta z/2 \tag{30}$$

$$(P_5 - P_4)_{(1)} = (P_5 - P_6)_{(1)} = g \cdot \delta\rho \cdot \delta z/2 \tag{31}$$

These pressures result in forces which would tend to split the particles causing flow to both sides. Assuming that the kinetic energy per unit volume associated with lateral motion is equal to the potential energy per unit volume associated with (and equal to) the lateral pressure differences (pressure equivalent to potential energy per unit volume), the kinetic energy per unit volume is given by

$$W_F = -g \cdot \delta\rho \cdot \delta z \tag{32}$$

The total energy per unit volume required to interchange the particles is the buoyant work W_B (Eq. (26)) plus the kinetic energy per unit volume associated with the lateral pressure differences, W_F (Eq. (32)):

$$W_T = -2g \cdot \delta\rho \cdot \delta z \tag{33}$$

For instability to occur the kinetic energy per unit volume, E, available from the shear (Eq. (27)) must be greater than the total energy per unit volume, W_T:

$$\frac{W_T}{E} = -\frac{2g \cdot \delta\rho \cdot \delta z}{\rho(\delta V)^2/4} < 1.0 \tag{34}$$

The critical Richardson number is obtained by dividing the numerator and denominator in Eq. (34) by δz:

$$-\frac{g(\delta\rho/\delta z)}{\rho(\delta V/\delta z)^2} = Ri < 0.125 \tag{35}$$

Thus, for three-dimensional, stably, stratified, shear flows one would expect instability to occur only when the Richardson number was less than 0.125. On the basis of this result, then, "three-dimensional" flows would be more stable than two-dimensional flows which have a critical Richardson number of 0.25. This result is confirmed to some degree by experimental results obtained during this program and discussed previously.

SKETCH OF UARL OPEN WATER CHANNEL

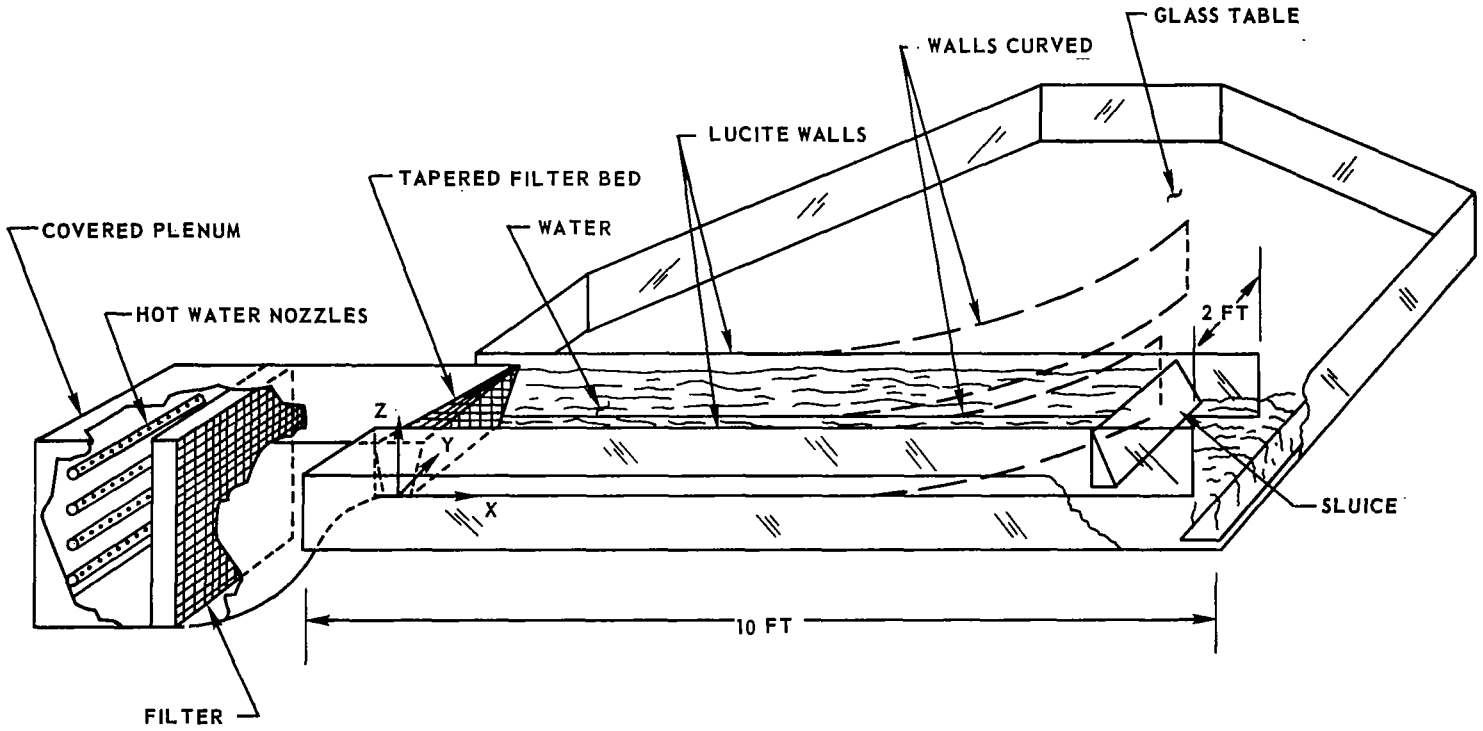

FIG. 1

COMPARISON OF WATER CHANNEL RESULTS FOR HYPERBOLIC TANGENT VELOCITY PROFILES WITH DRAZIN'S CRITERION FOR STABILITY

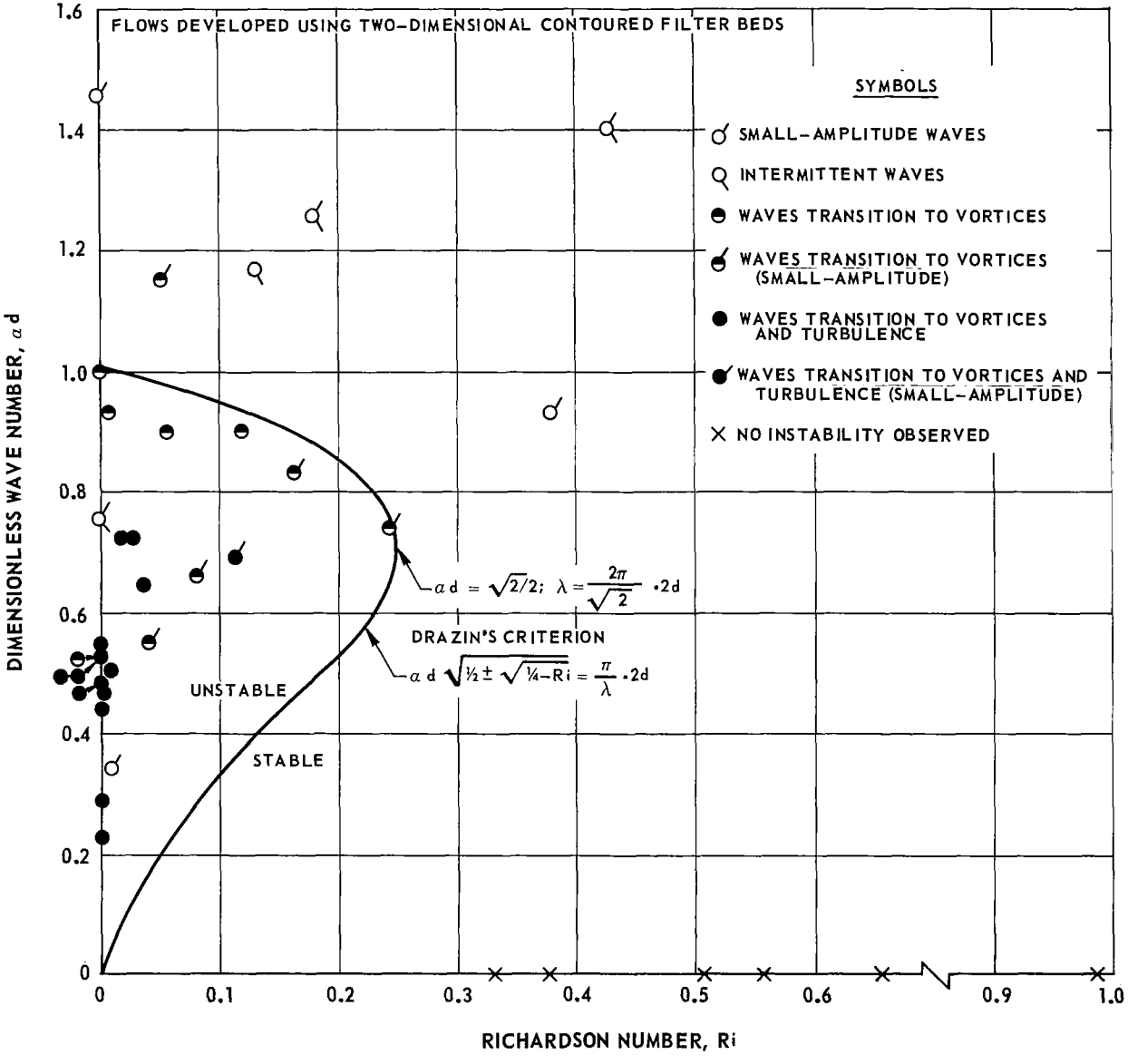

FIG. 2

FIG. 3

TYPICAL STAGES OF BREAKDOWN OF FLOW IN SHEAR LAYERS HAVING "S-SHAPED" VELOCITY PROFILES

V_o = 0.07 FT/SEC $\quad (\partial V/\partial z)_o = -0.80$ SEC^{-1} $\quad (\partial T/\partial z)_o = 0$

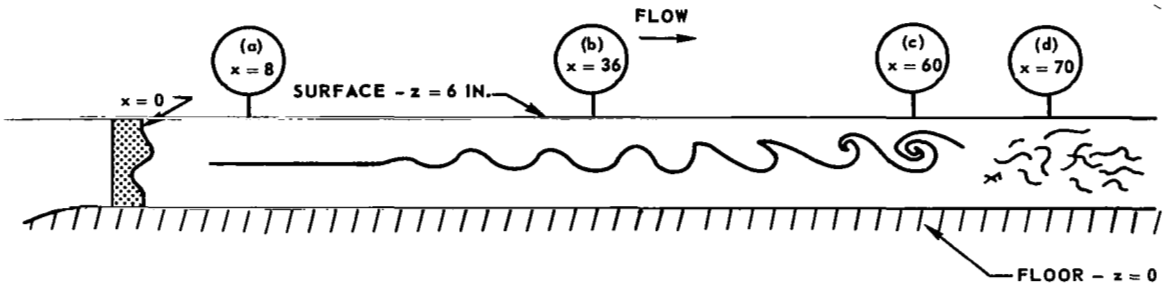

(a) x = 8 IN. – UNDISTURBED

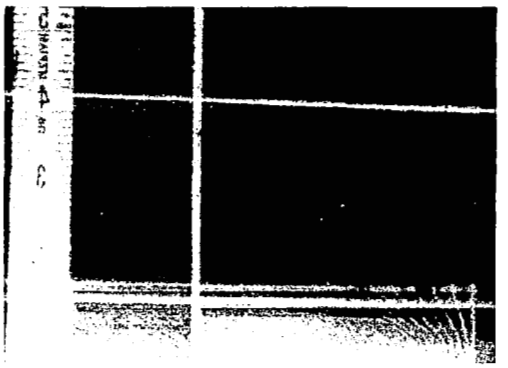

(b) x = 36 IN. – WAVES

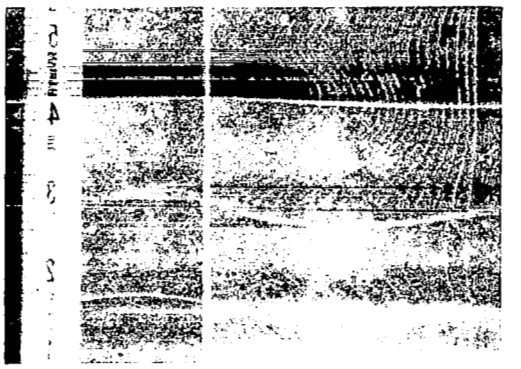

(c) x = 60 IN. – VORTICES

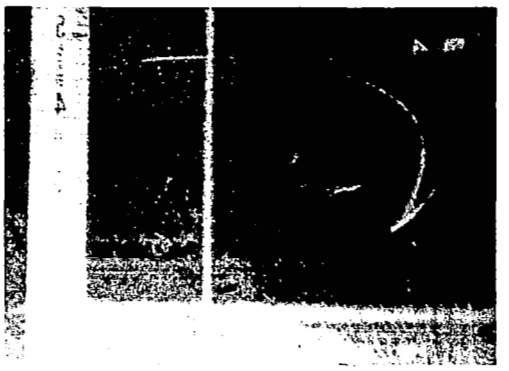

(d) x = 70 IN. – TURBULENCE

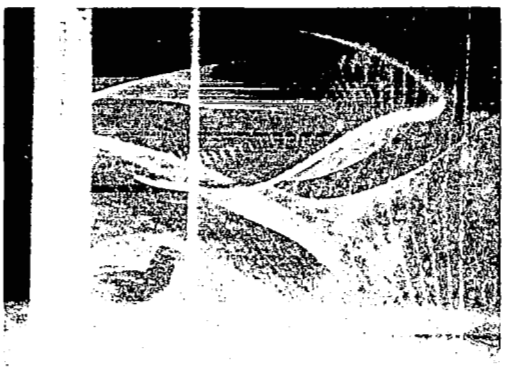

FIG. 4

TYPICAL "S" VELOCITY, TEMPERATURE AND DENSITY PROFILES FOR SHEAR-FLOW EXPERIMENTS IN WATER CHANNEL

— — CORRESPONDING PROFILE IN HAZEL'S THEORY
SEE EQS. (6) AND (8) FOR THEORETICAL VELOCITY AND DENSITY PROFILES

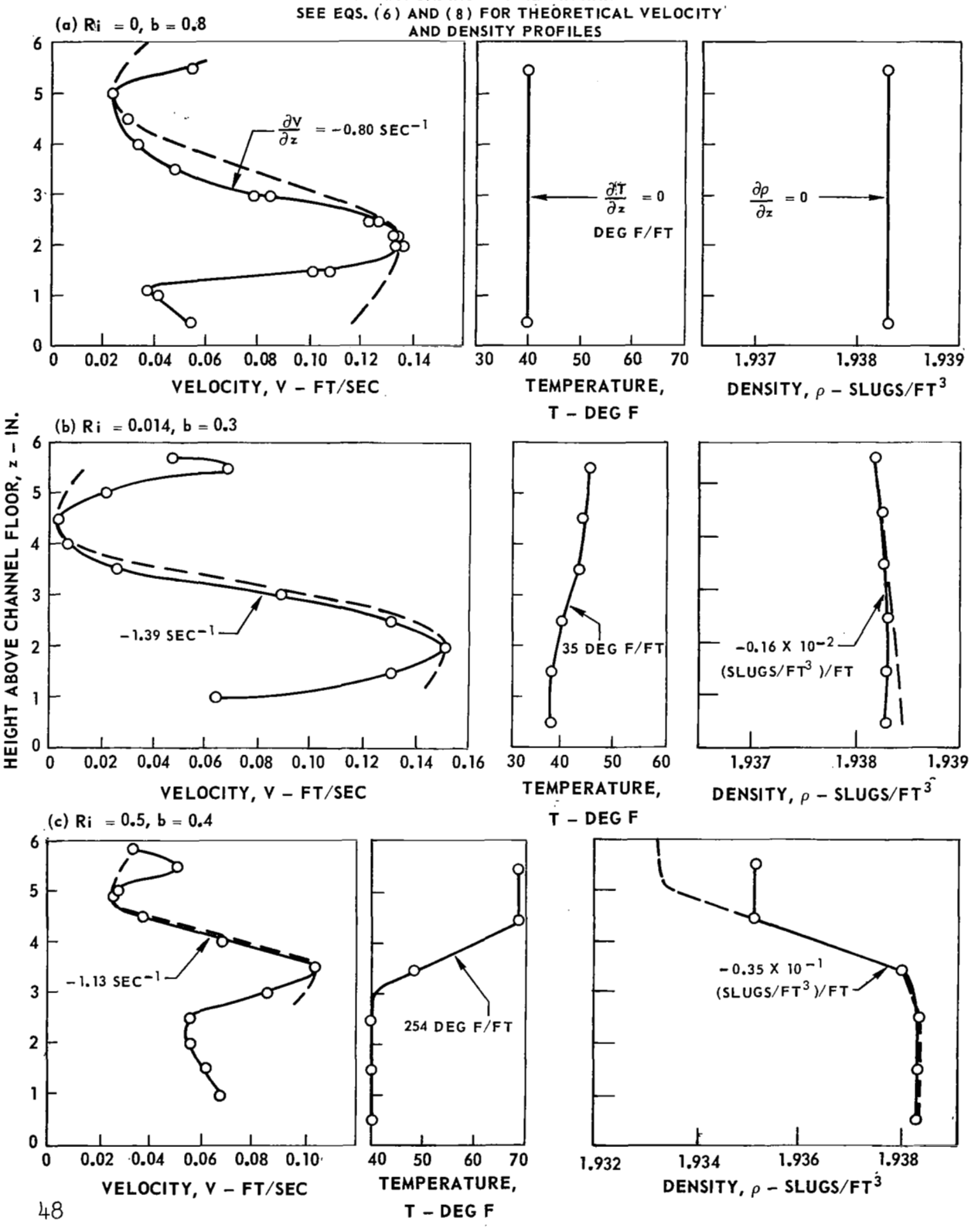

FIG. 5

COMPARISON OF WATER CHANNEL RESULTS FOR "S-SHAPED" VELOCITY PROFILES WITH HAZEL'S CRITERIA FOR STABILITY

FLOW DEVELOPED USING TWO-DIMENSIONAL CONTOURED FILTER BEDS
SEE EQS. (6) AND (8) FOR THEORETICAL VELOCITY AND DENSITY PROFILES

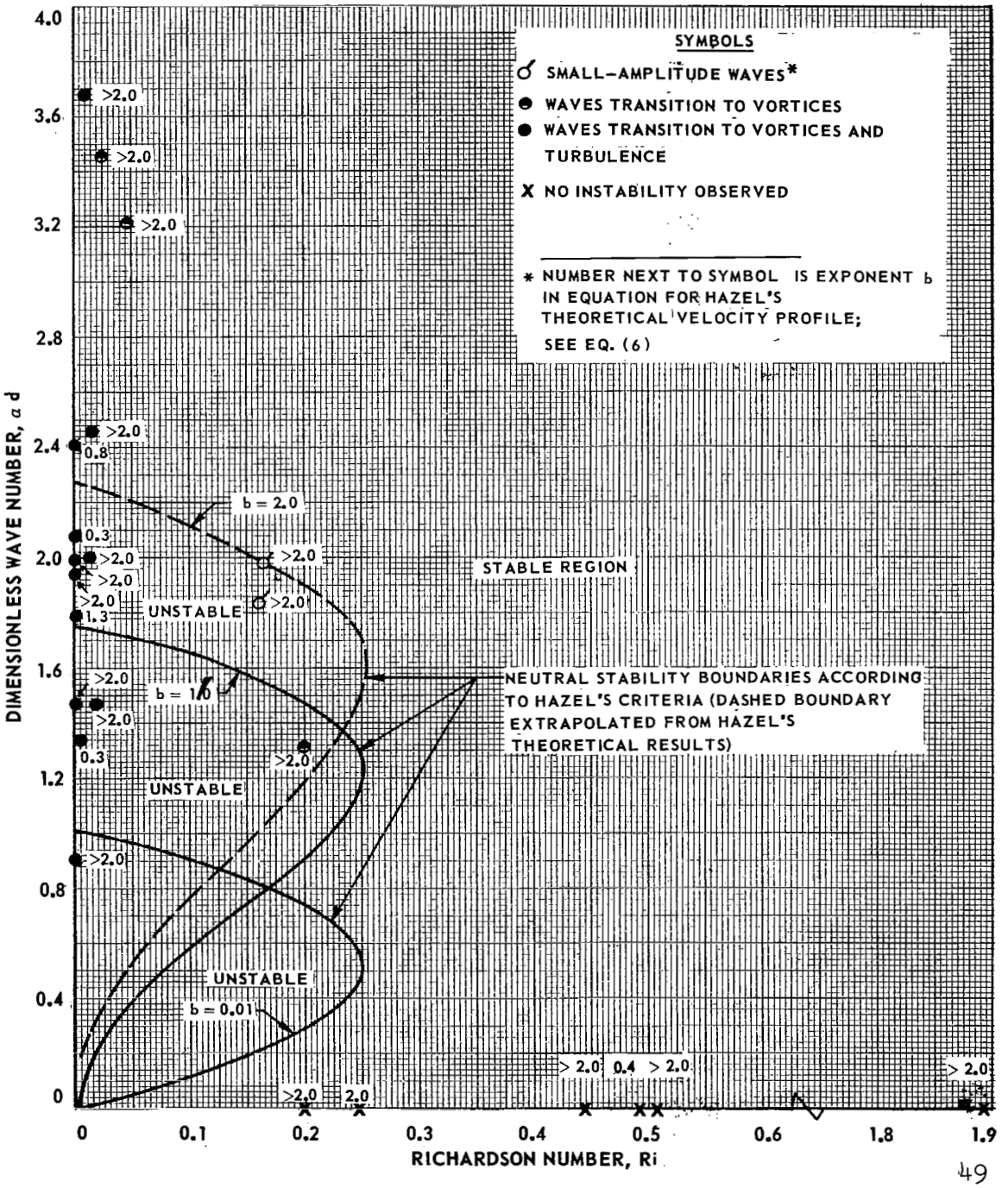

PHOTOGRAPH OF FILTER BED FOR DEVELOPING VELOCITY PROFILES WHICH VARY ACROSS THE CHANNEL

ALL DIMENSIONS APPROXIMATE

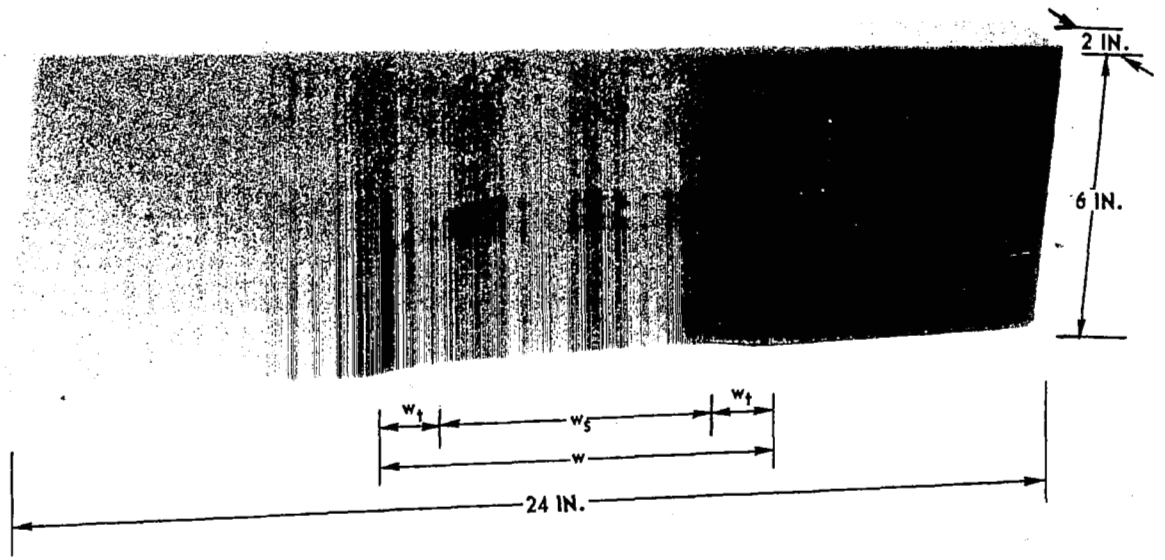

FIG. 6

FIG. 7

TYPICAL STAGES OF BREAKDOWN OF FLOW IN SHEAR LAYERS HAVING "THREE-DIMENSIONAL" VELOCITY PROFILES

V_o = 0.07 FT/SEC $\quad \partial V/\partial z = -2.2$ SEC^{-1} $\quad \partial T/\partial z = 0$

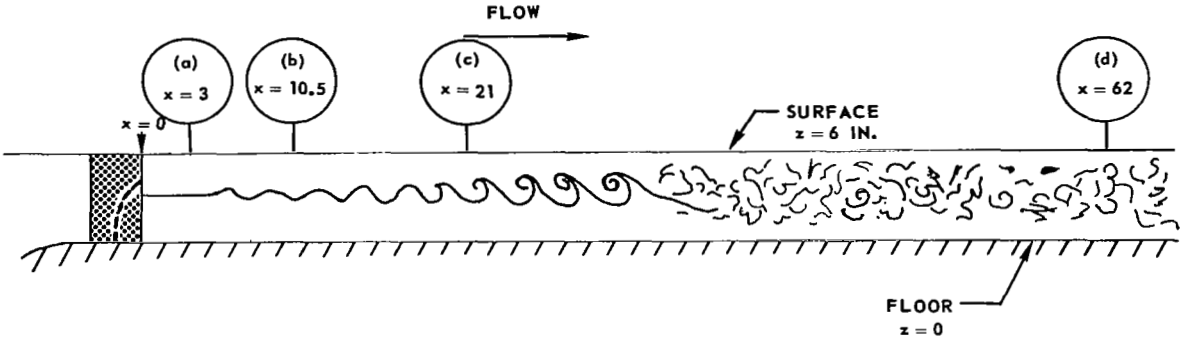

(a) x = 3 IN. – UNDISTURBED

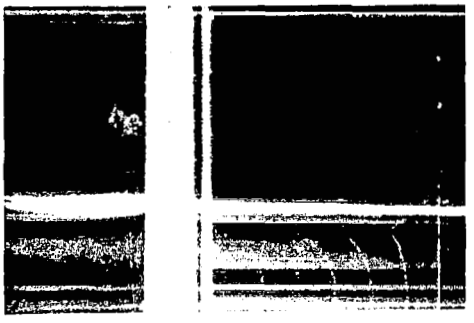

(b) x = 10.5 IN. – WAVES

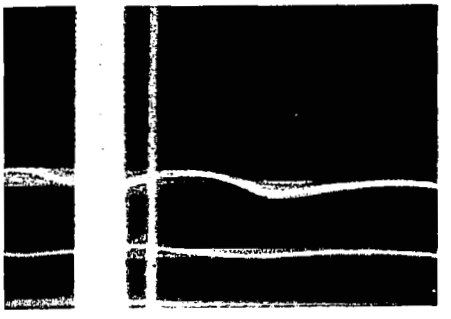

(c) x = 21 IN. – VORTICES

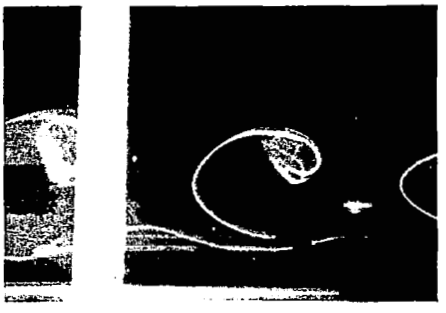

(d) x = 62 IN. – TURBULENCE

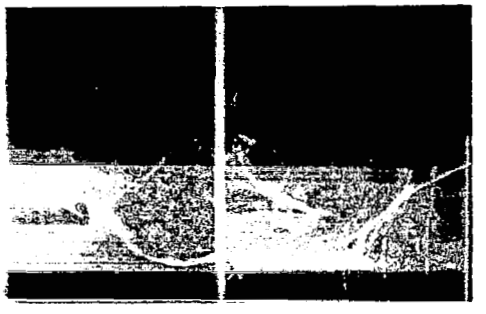

FIG. 8

TYPICAL VELOCITY, TEMPERATURE AND DENSITY PROFILES FOR "THREE-DIMENSIONAL" SHEAR-FLOW EXPERIMENTS

ALL MEASUREMENTS 2 IN. DOWNSTREAM FROM TAPERED FILTER BED AT CENTER OF CHANNEL

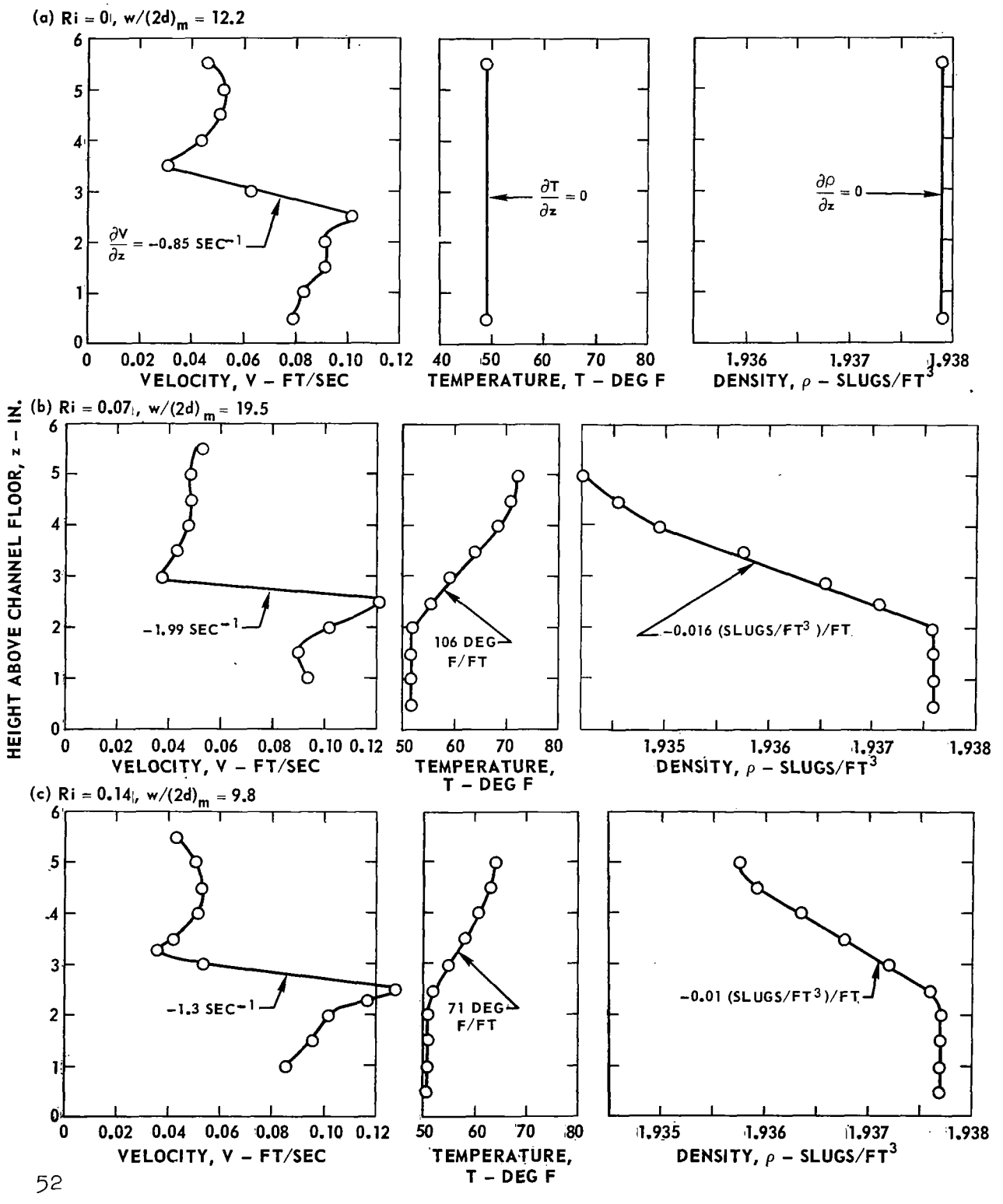

FIG. 9

COMPARISON OF RESULTS FOR FLOWS HAVING "THREE-DIMENSIONAL" SHEAR LAYER WIDTH-TO-THICKNESS RATIOS BETWEEN 4.8 AND 8.6 WITH DRAZIN'S CRITERION FOR TWO-DIMENSIONAL FLOWS

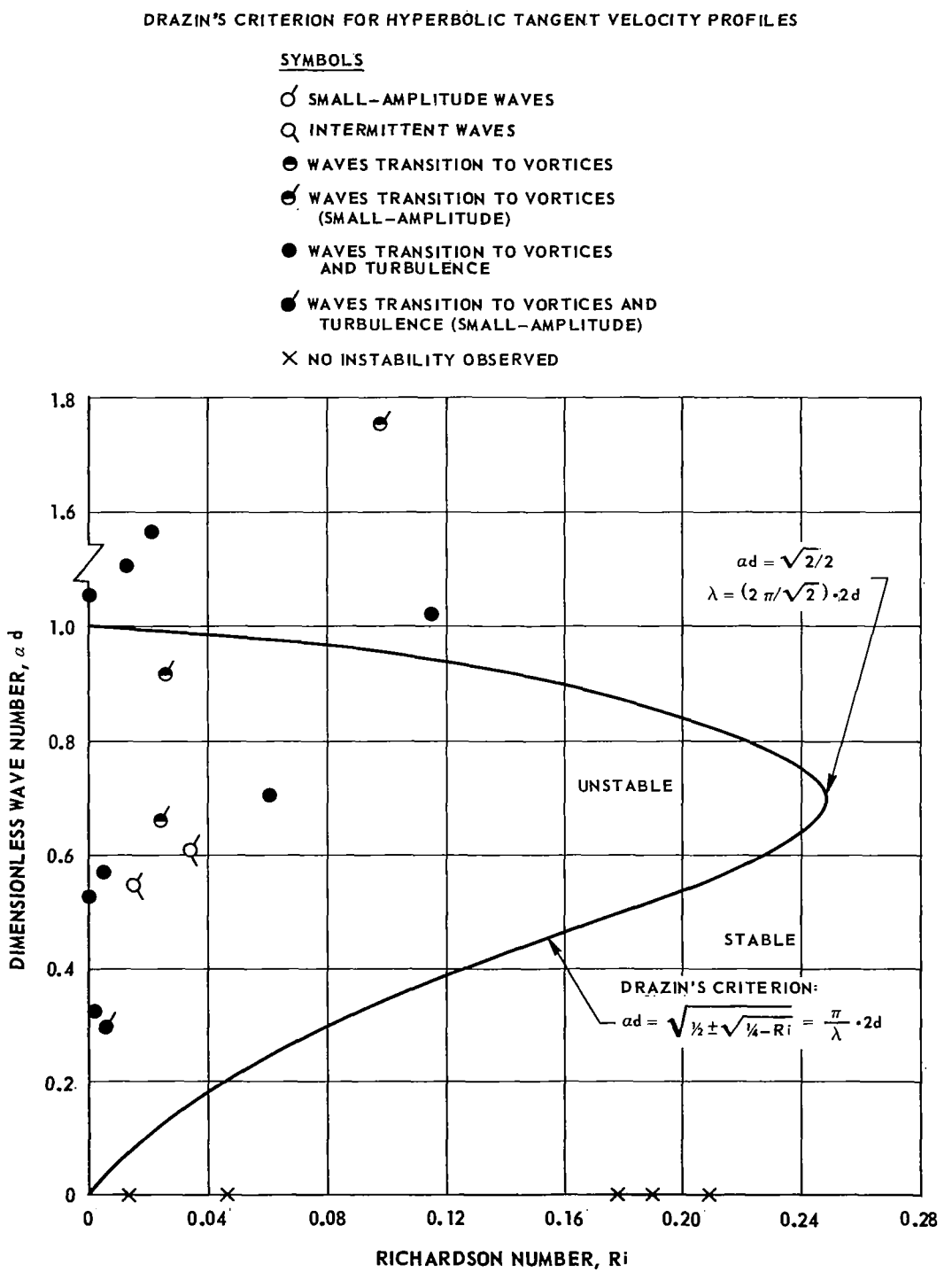

FIG. 10

COMPARISON OF RESULTS FOR FLOWS HAVING "THREE-DIMENSIONAL" SHEAR LAYER WIDTH-TO-THICKNESS RATIOS BETWEEN 9.7 AND 14.3 WITH DRAZIN'S CRITERION FOR TWO-DIMENSIONAL FLOWS

DRAZIN'S CRITERION FOR HYPERBOLIC TANGENT VELOCITY PROFILES

SYMBOLS

- SMALL-AMPLITUDE WAVES
- INTERMITTENT WAVES
- WAVES TRANSITION TO VORTICES
- WAVES TRANSITION TO VORTICES (SMALL-AMPLITUDE)
- WAVES TRANSITION TO VORTICES (INTERMITTENT)
- WAVES TRANSITION TO VORTICES AND TURBULENCE
- NO INSTABILITY OBSERVED

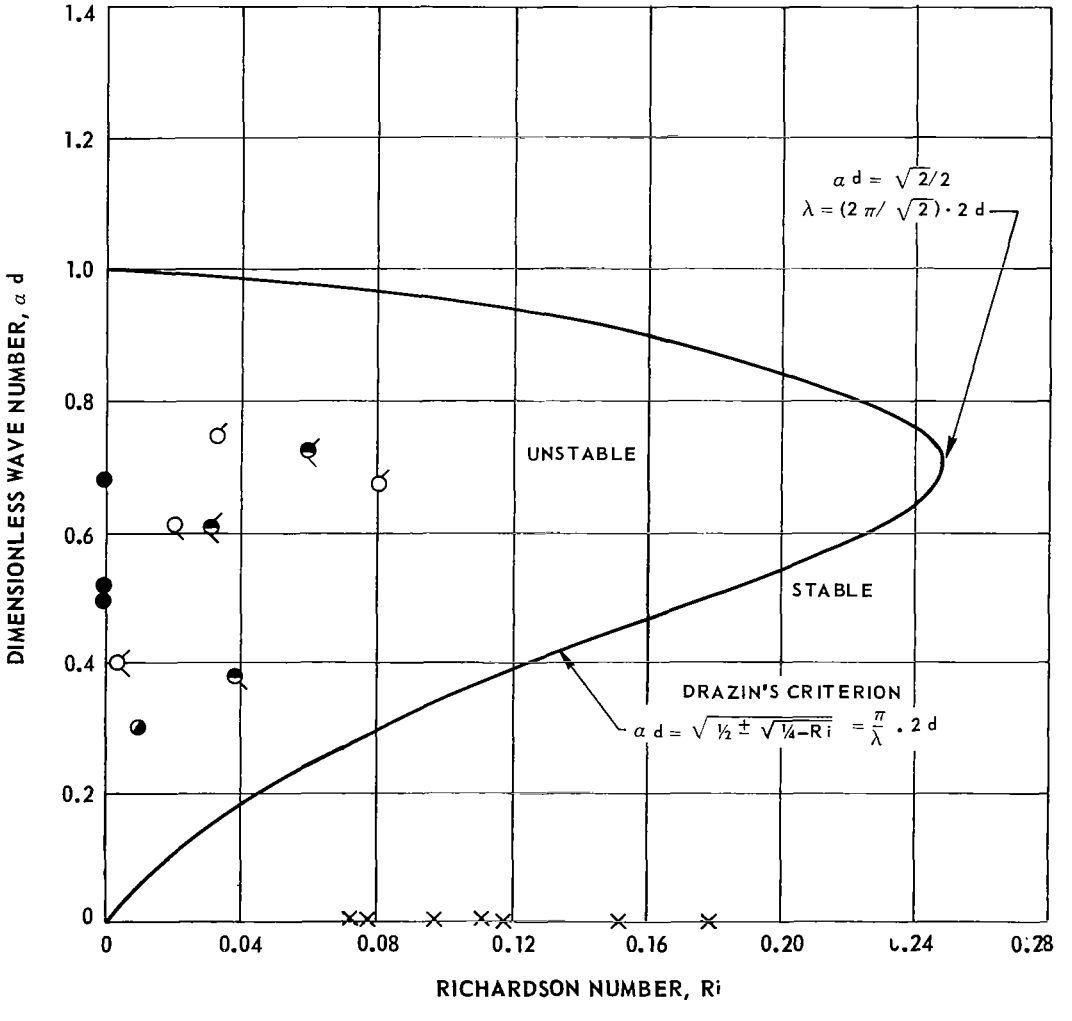

FIG. 11

COMPARISON OF RESULTS FOR FLOWS HAVING "THREE-DIMENSIONAL" SHEAR LAYER WIDTH-TO-THICKNESS RATIOS BETWEEN 14.5 AND 40 WITH DRAZIN'S CRITERION FOR TWO-DIMENSIONAL FLOWS

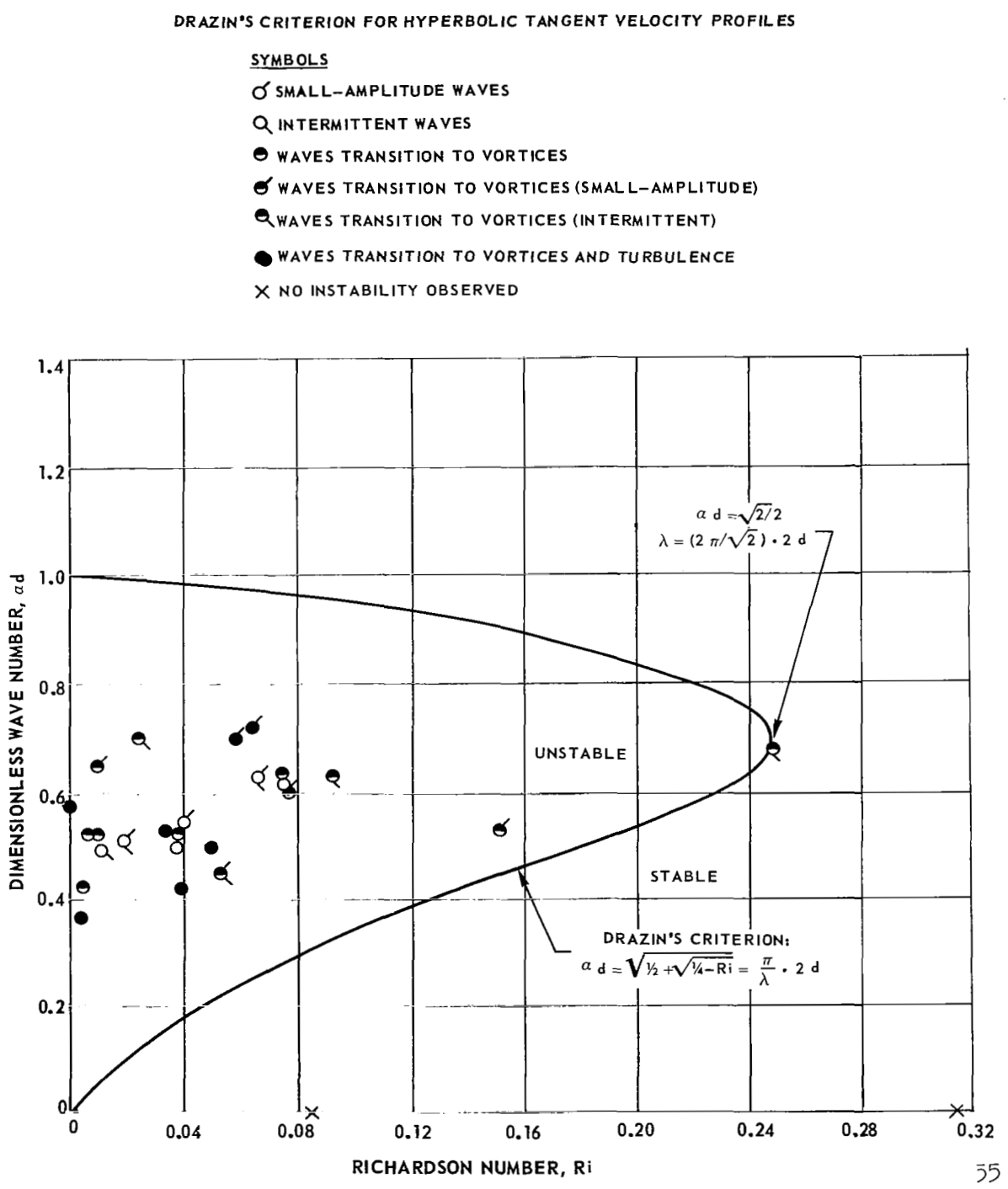

EFFECT OF RATIO OF WIDTH TO THICKNESS OF SHEAR LAYER ON STABILITY OF "THREE-DIMENSIONAL" FLOWS

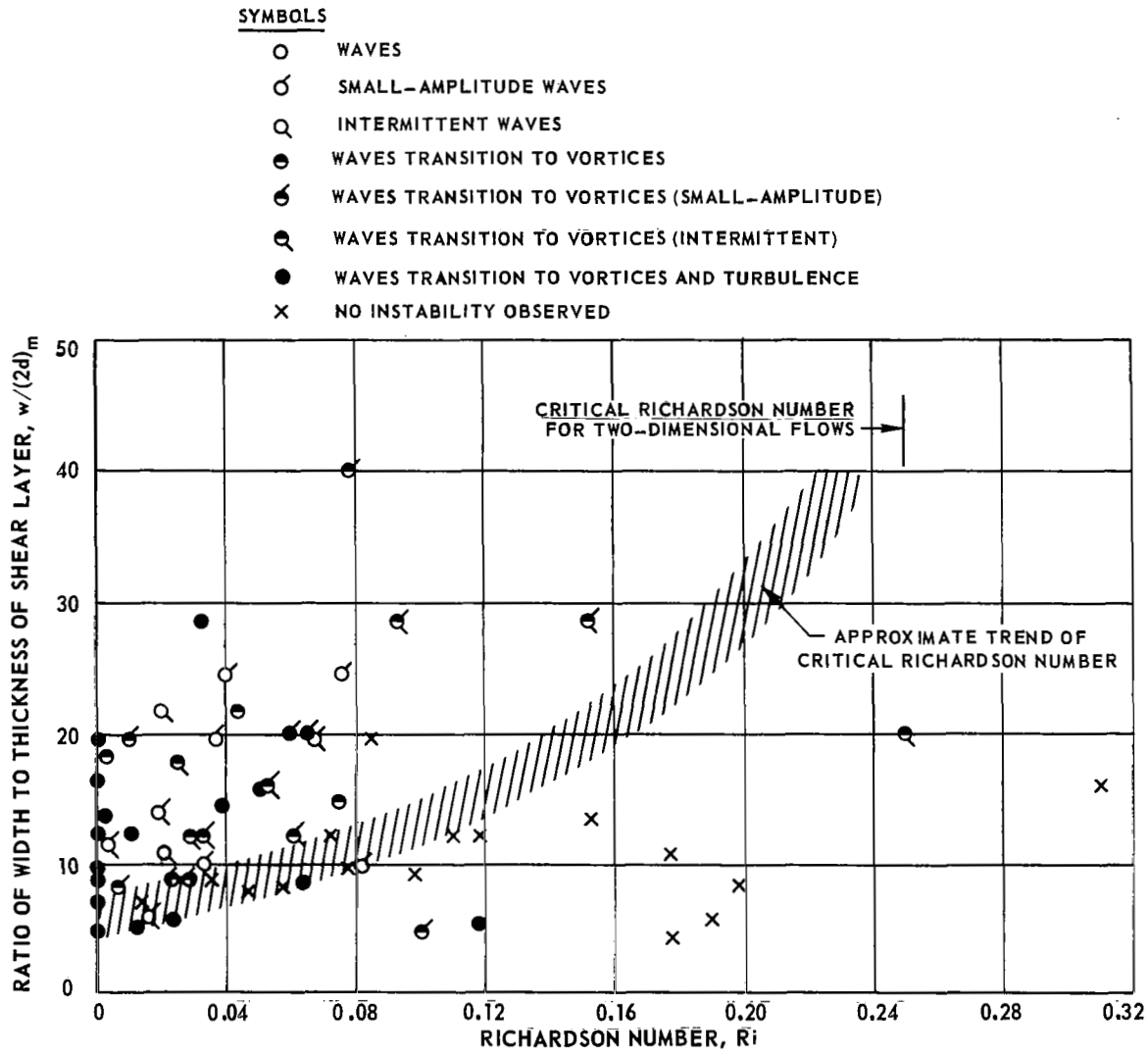

FIG. 12

FIG. 13

EFFECT OF A LONG-WAVELENGTH WAVE ON THE MINIMUM RICHARDSON NUMBER IN A SHEAR FLOW

(a) SCHEMATIC DIAGRAM OF FLOW CONDITION

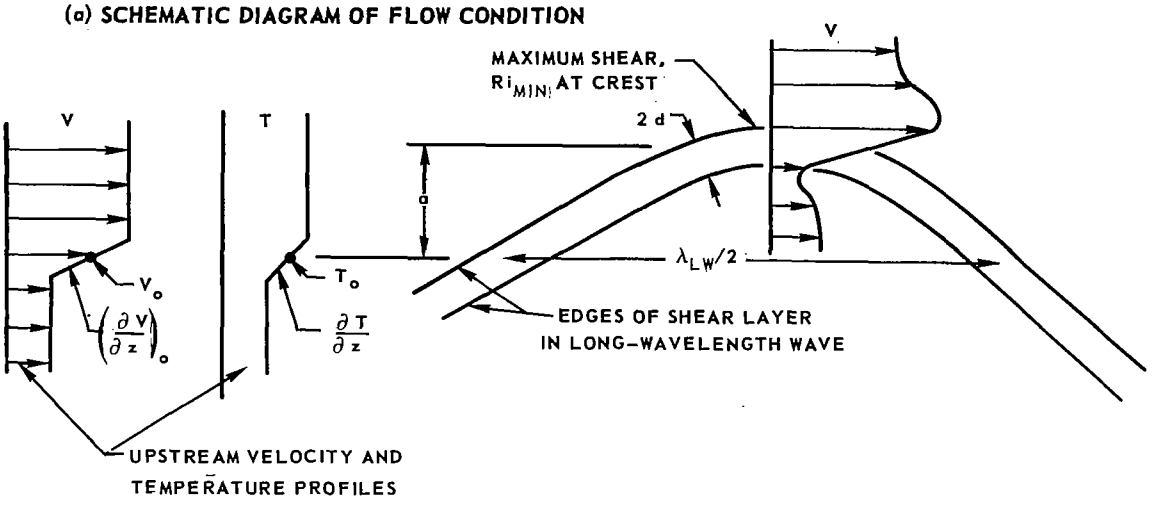

(b) EFFECT OF TEMPERATURE GRADIENT AND INITIAL SHEAR ON Ri_{MIN} IN WATER

$$Ri_{MIN} = \frac{N_M^2}{\left[\left|\left(\frac{\partial V}{\partial z}\right)_o\right| + (N_M^2 - n^2)\cdot\frac{a}{V_o}\right]^2}$$

$V_o = 0.10$ FT/SEC

$T_o = 60$ DEG F

$a = 0.05$ FT

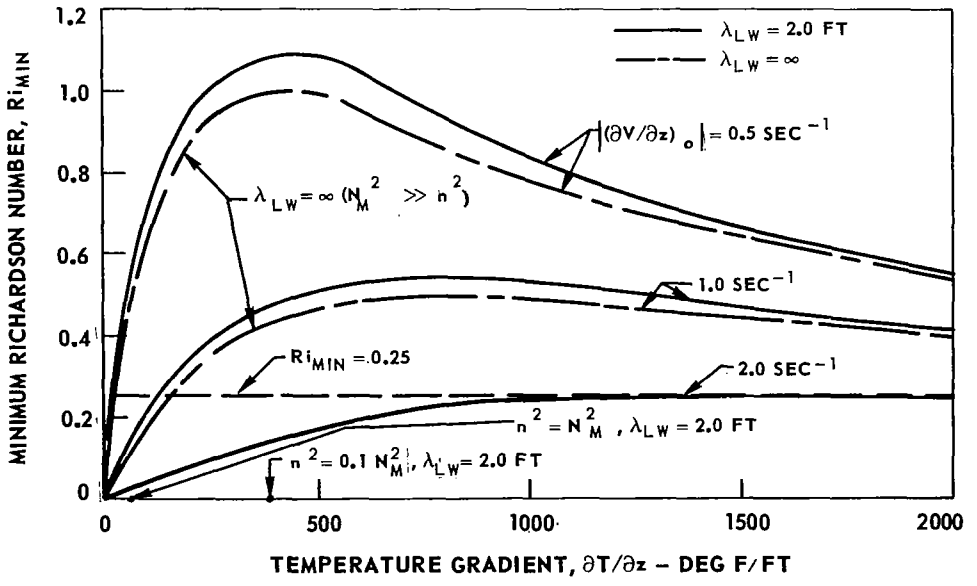

FIG. 14

WATER CHANNEL RESULTS SHOWING EFFECT OF A LONG-WAVELENGTH WAVE ON THE LOCAL RICHARDSON NUMBER IN A SHEAR FLOW

V_o = 0.07 FT/SEC Ri_o = 0.70 $(\partial V/\partial z)_o$ = −0.71 SEC^{-1}

SEE FIG. 16 FOR VELOCITY, TEMPERATURE AND DENSITY PROFILES

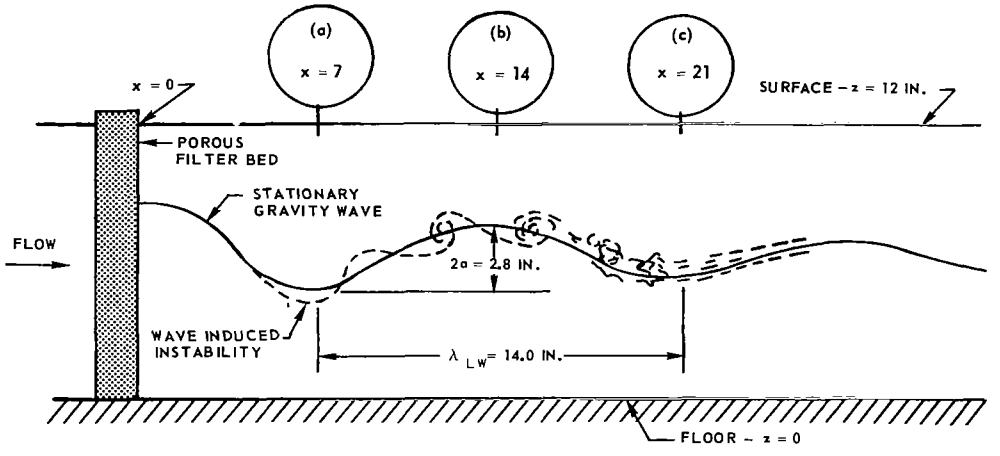

(a) x = 7 IN.–TROUGH

$\partial V/\partial z = -1.03\ SEC^{-1}$, $\partial T/\partial z$ = 120 DEG F/FT

Ri = 0.37

(b) x = 14 IN.–CREST

$\partial V/\partial z = 0.39\ SEC^{-1}$, $\partial T/\partial z$ = 82 DEG F/FT

Ri = 1.8

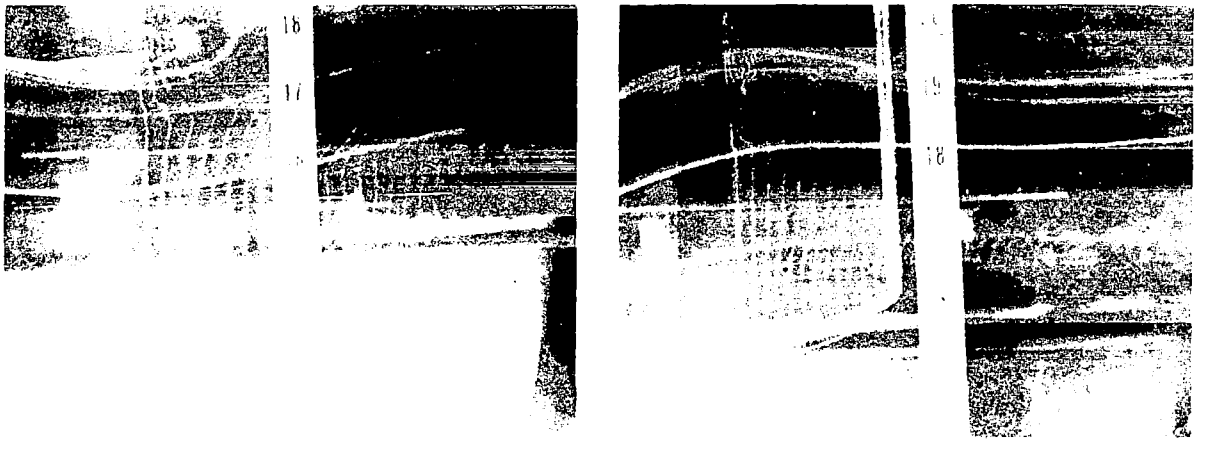

FIG.15

PHOTOGRAPHS SHOWING EXAMPLES OF INSTABILITIES INDUCED BY LONG-WAVELENGTH WAVES

SEE FIG. 14 FOR FLOW CONDITIONS AND FIG. 16 FOR VELOCITY, TEMPERATURE, AND DENSITY PROFILES

DIRECTION OF FLOW →

(a) FIRST TROUGH TO SECOND CREST (X=7 TO 14 IN.)–WAVES

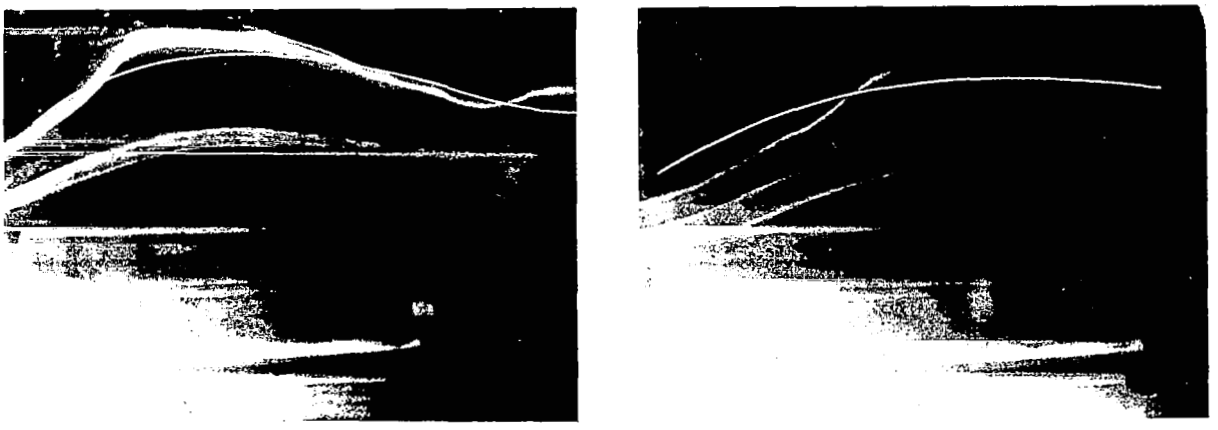

(b) SECOND CREST TO SECOND TROUGH (X= 14 TO 21 IN.)– VORTICES

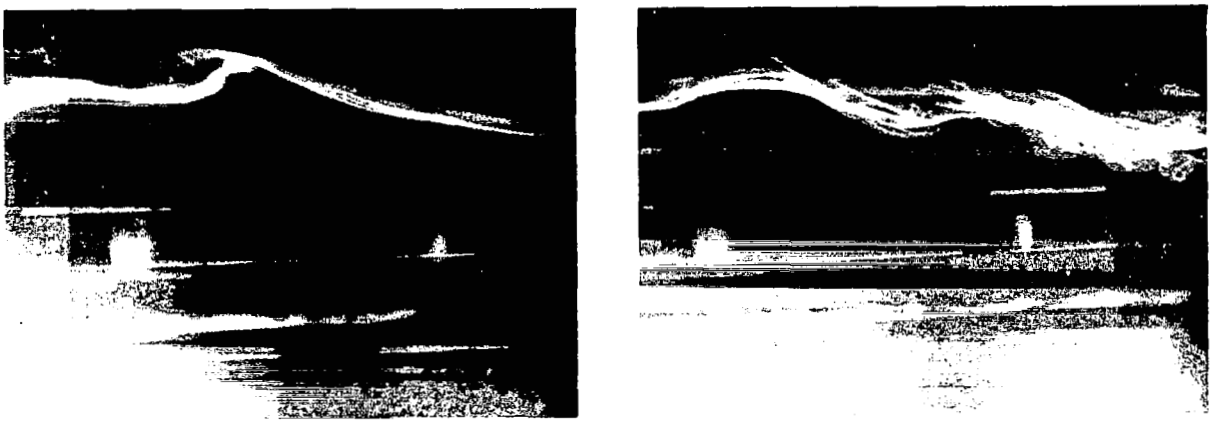

FIG. 16

TYPICAL VELOCITY, TEMPERATURE AND DENSITY PROFILES FOR FLOW IN A LONG-WAVELENGTH WAVE

SEE FIGS. 14 AND 15 FOR PHOTOGRAPHS OF THE FLOW

$V_o = 0.07$ FT/SEC, $(\partial V/\partial z)_o = -0.71\ SEC^{-1}$, $\lambda_{LW} = 14$ IN., $a = 1.4$ IN.

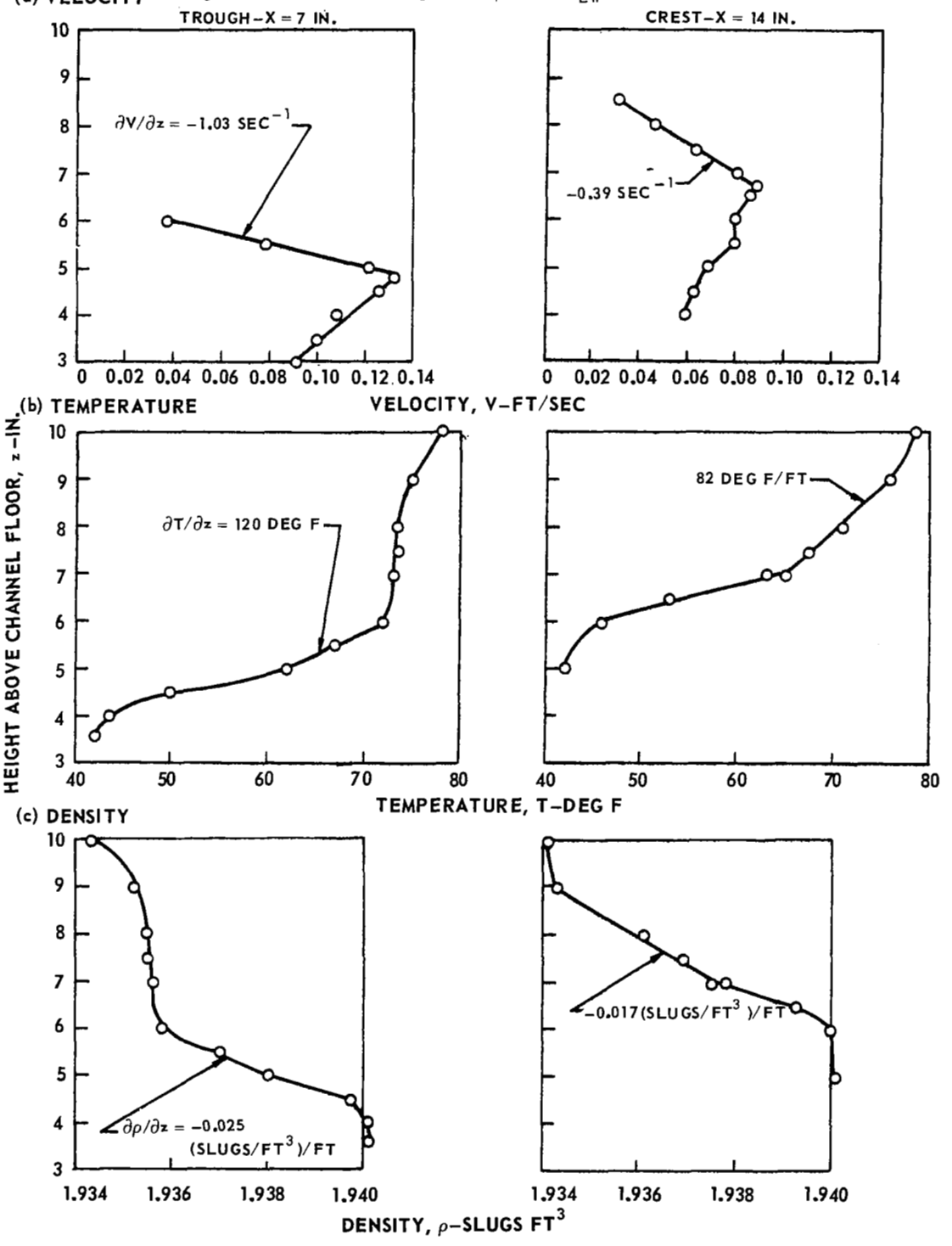

FIG. 17

COMPARISON BETWEEN MEASURED AND PREDICTED VALUES OF WAVE SHEAR IN A LONG-WAVELENGTH WAVE

SHEAR PREDICTED USING PHILLIPS' THEORY (REF. 9)

$$\left|\Delta\,(\partial V/\partial z)\right|_p = (a/V_O)\,(N_M^2 - n^2)$$

MEASURED WAVE SHEAR GENERALLY BASED ON FIRST HALF WAVELENGTH OF LONG-WAVELENGTH WAVE

DATA FROM UARL OPEN WATER CHANNEL

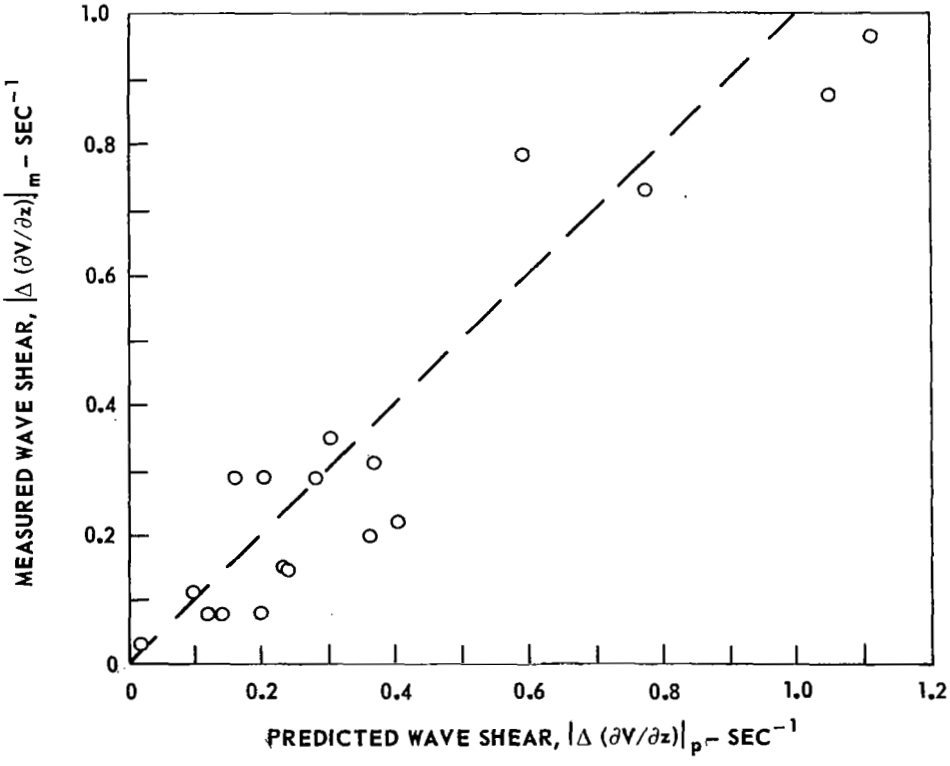

FIG. 18

COMPARISON BETWEEN MEASURED AND PREDICTED VALUES OF WAVELENGTH OF LONG-WAVELENGTH WAVES

DATA FROM UARL OPEN WATER CHANNEL

WAVELENGTH PREDICTED USING HAURWITZ'S THEORY (REF. 10)

$$\left(\lambda_{LW}\right)_P = \frac{2\pi}{g}\,\frac{\rho_2\, V_2^{\,2}}{(\rho_2 - \rho_1)}\left[\left(\frac{V_1}{V_2}\right)^2 \frac{\rho_1}{\rho_2} + 1\right]$$

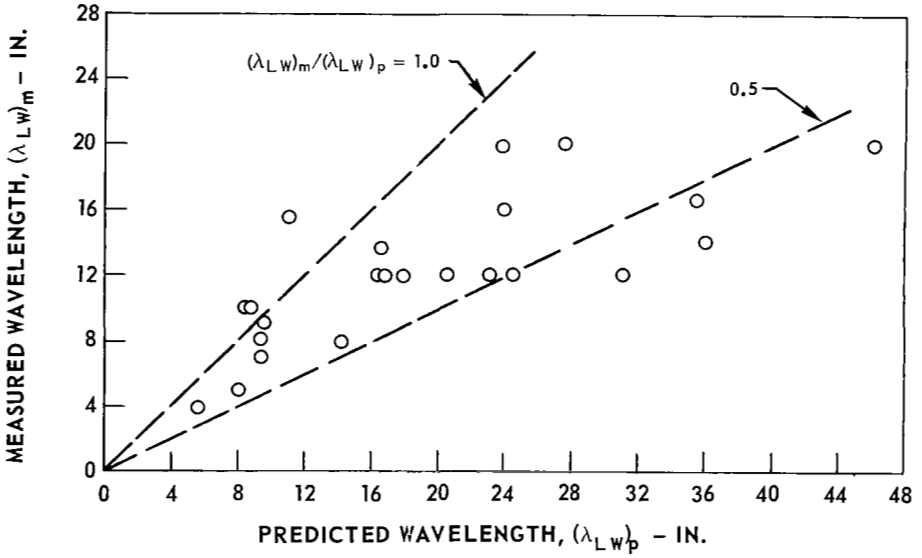

FIG. 19

EFFECT OF WAVE AMPLITUDE RATIO ON STABILITY BOUNDARIES FOR SHEAR FLOWS IN LONG-WAVELENGTH WAVES

DATA FROM UARL OPEN WATER CHANNEL

SYMBOL	LONG-WAVELENGTH WAVE OBSERVED?
○ a/V_o	YES
●	NO

LETTER	INSTABILITY OBSERVED
W	WAVES
V	VORTICES
T	TURBULENCE

$$\Delta\left(\frac{\partial V}{\partial z}\right) = N_M^2\left(\frac{a}{V_o}\right)$$

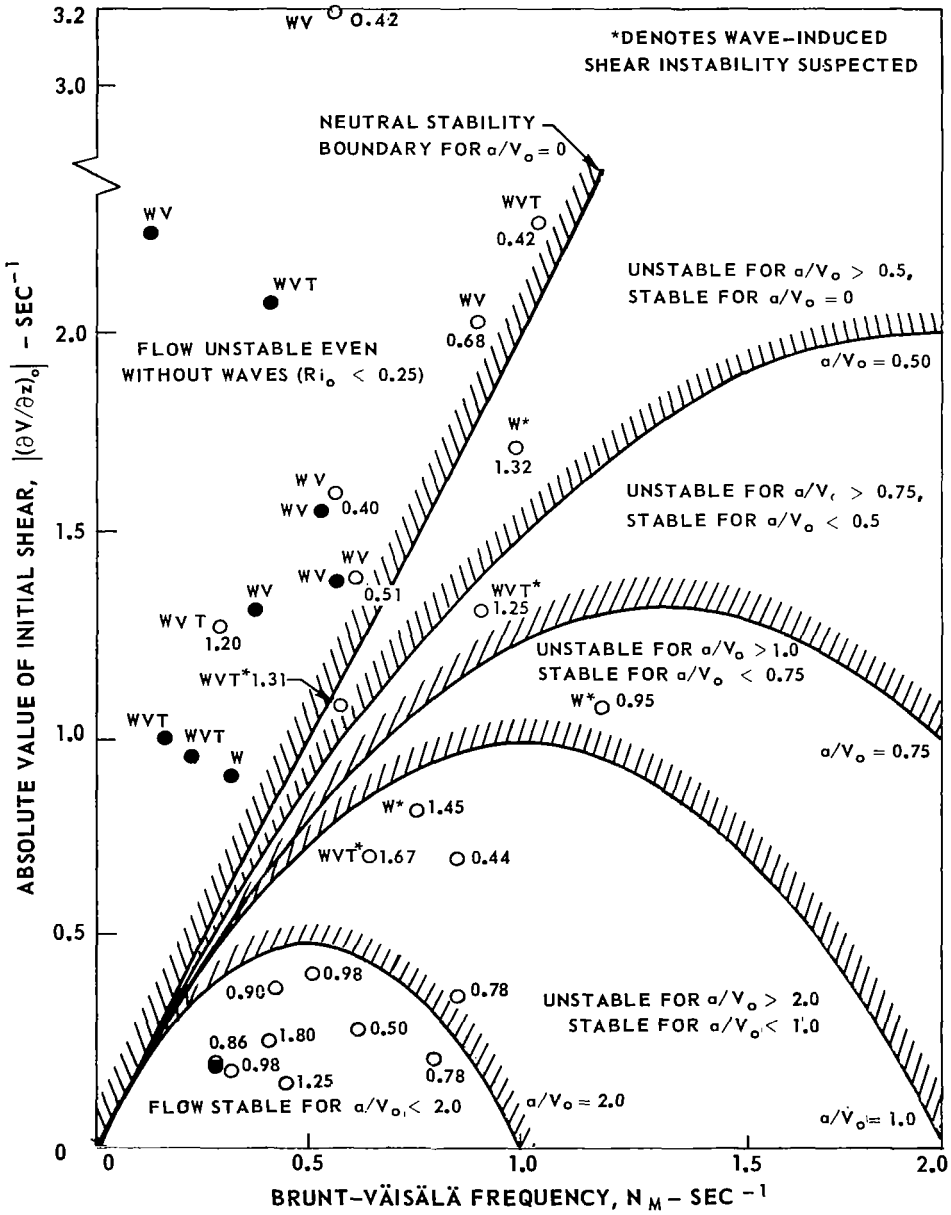

FIG. 20

EFFECTS OF LONG-WAVELENGTH WAVES ON STABILITY OF ATMOSPHERIC SHEAR LAYERS

(a) SCHEMATIC DIAGRAM OF FLOW CONDITION

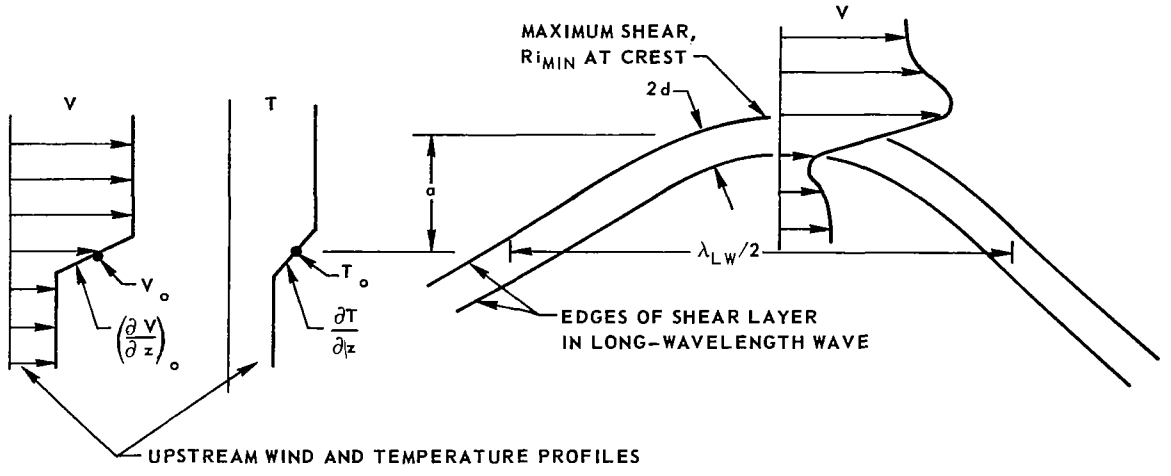

(b) EFFECT OF LAPSE RATE AND SHEAR ON Ri_{MIN} FOR TYPICAL WAVE CONDITIONS

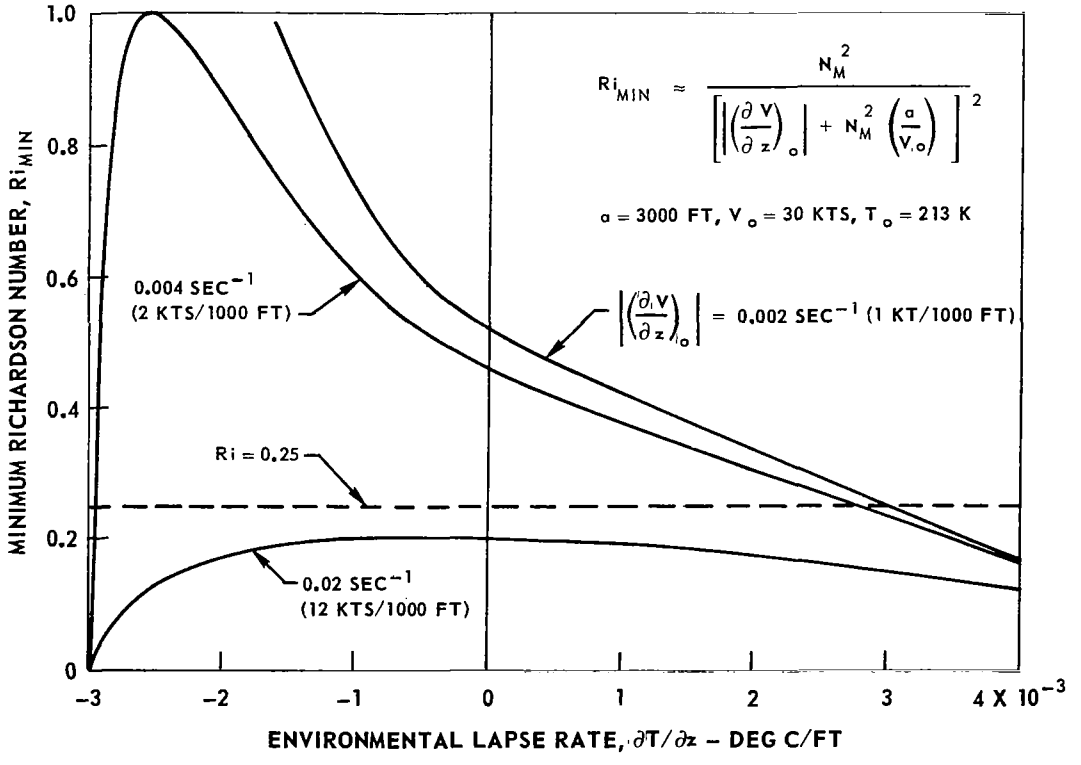

FIG. 21

EFFECT OF WIND VELOCITY ON STABILITY BOUNDARIES FOR ATMOSPHERIC SHEAR FLOWS IN A LONG-WAVELENGTH, 500-FT-AMPLITUDE WAVE

ALTITUDE, $z = 36{,}089$ FT

TEMPERATURE, $T_o = -56.5$ C

WAVELENGTH, $\lambda_{LW} = 15$ NMI

NOTE: FLOW STABLE FOR $|(\partial V/\partial z)_o|$ AND $\partial T/\partial z$ BELOW BOUNDARY FOR GIVEN V_o
AND UNSTABLE FOR $|(\partial V/\partial z)_o|$ AND $\partial T/\partial z$ ABOVE BOUNDARY

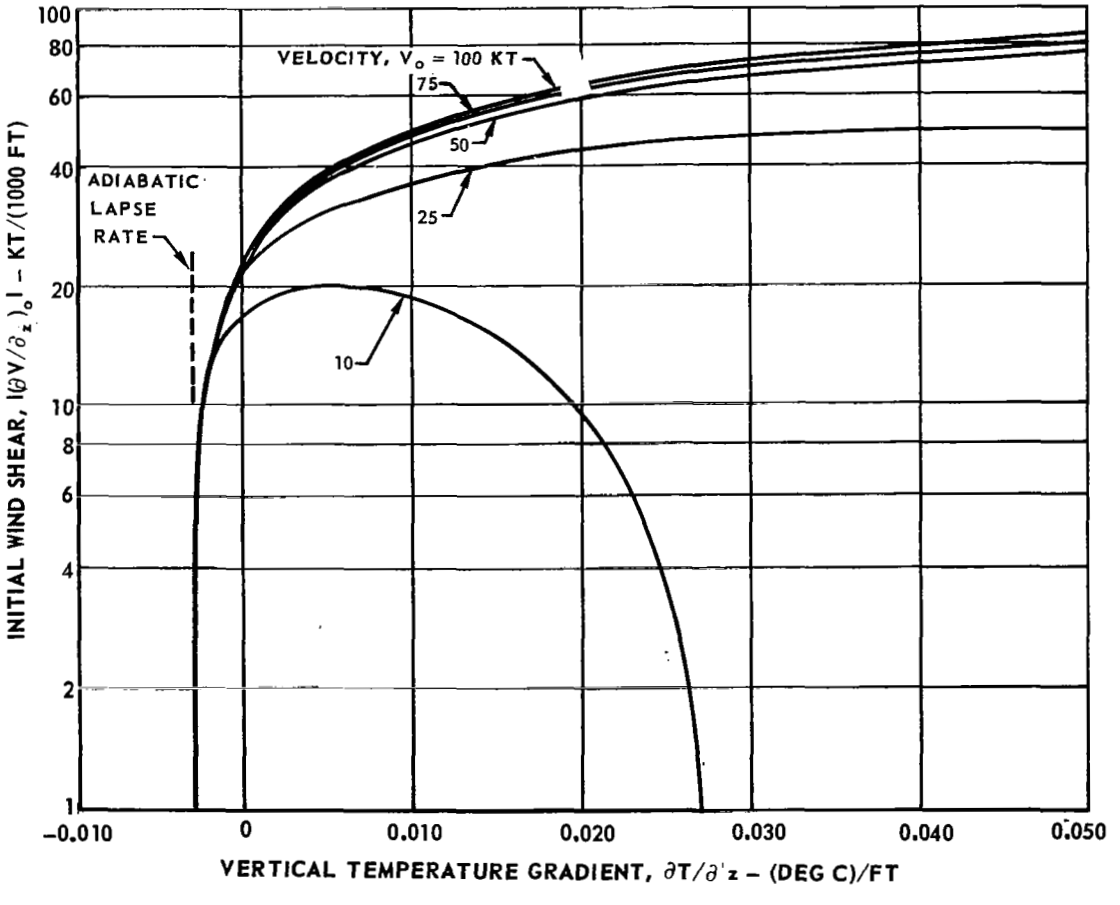

FIG. 22

EFFECT OF WIND VELOCITY ON STABILITY BOUNDARIES FOR ATMOSPHERIC SHEAR FLOWS IN A LONG–WAVELENGTH, 3000-FT-AMPLITUDE WAVE

ALTITIDE, $z = 36{,}089$ FT

TEMPERATURE, $T_o = -56.5$ C

WAVELENGTH, $\lambda_w = 15$ NMI

NOTE: FLOW STABLE FOR $|(\partial V/\partial z)_o|$ AND $\partial T/\partial z$ BELOW BOUNDARY FOR GIVEN V_o AND UNSTABLE FOR $|(\partial V/\partial z)_o|$ AND $\partial T/\partial z$ ABOVE BOUNDARY

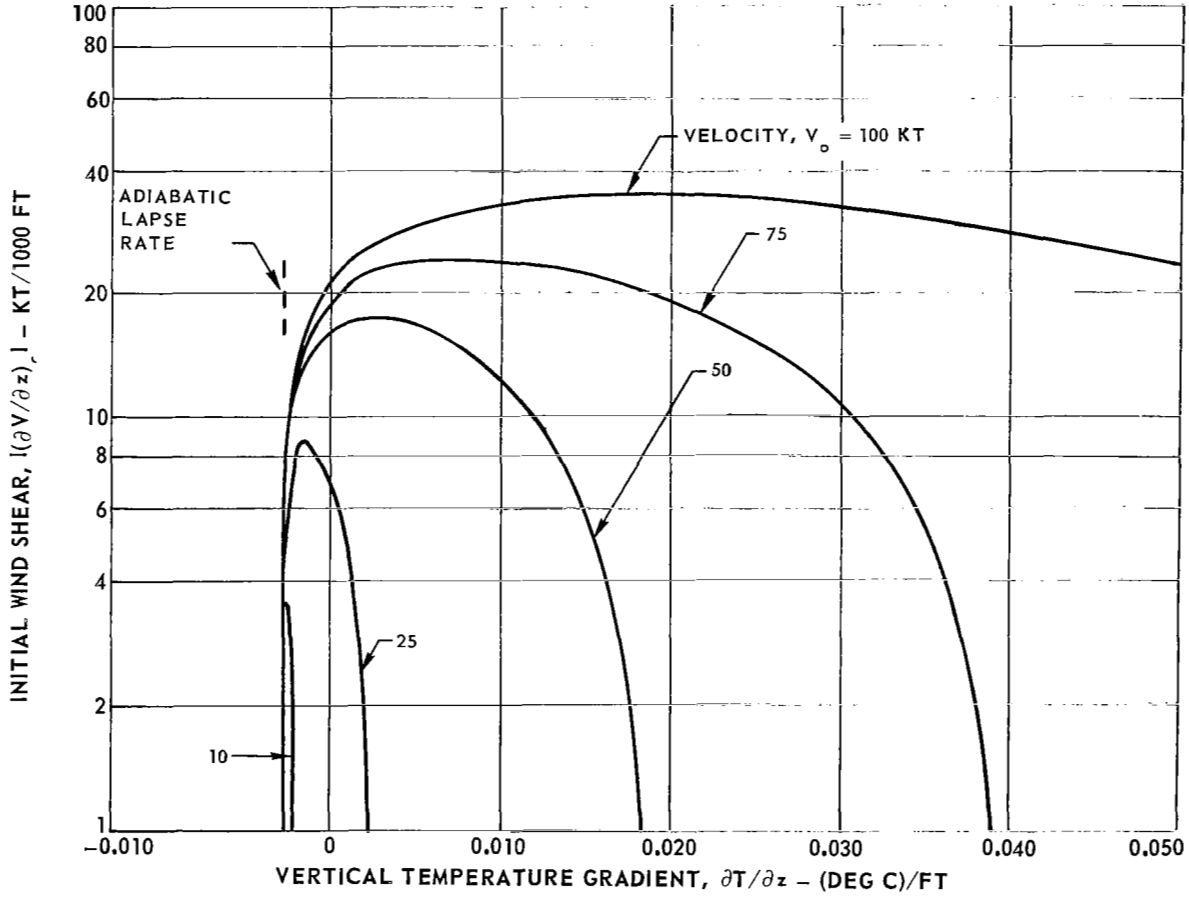

FIG. 23

EFFECTS OF WIND SPEED AND LONG-WAVE WAVELENGTH ON MAXIMUM ALLOWABLE INITIAL WIND SHEAR FOR STABILITY

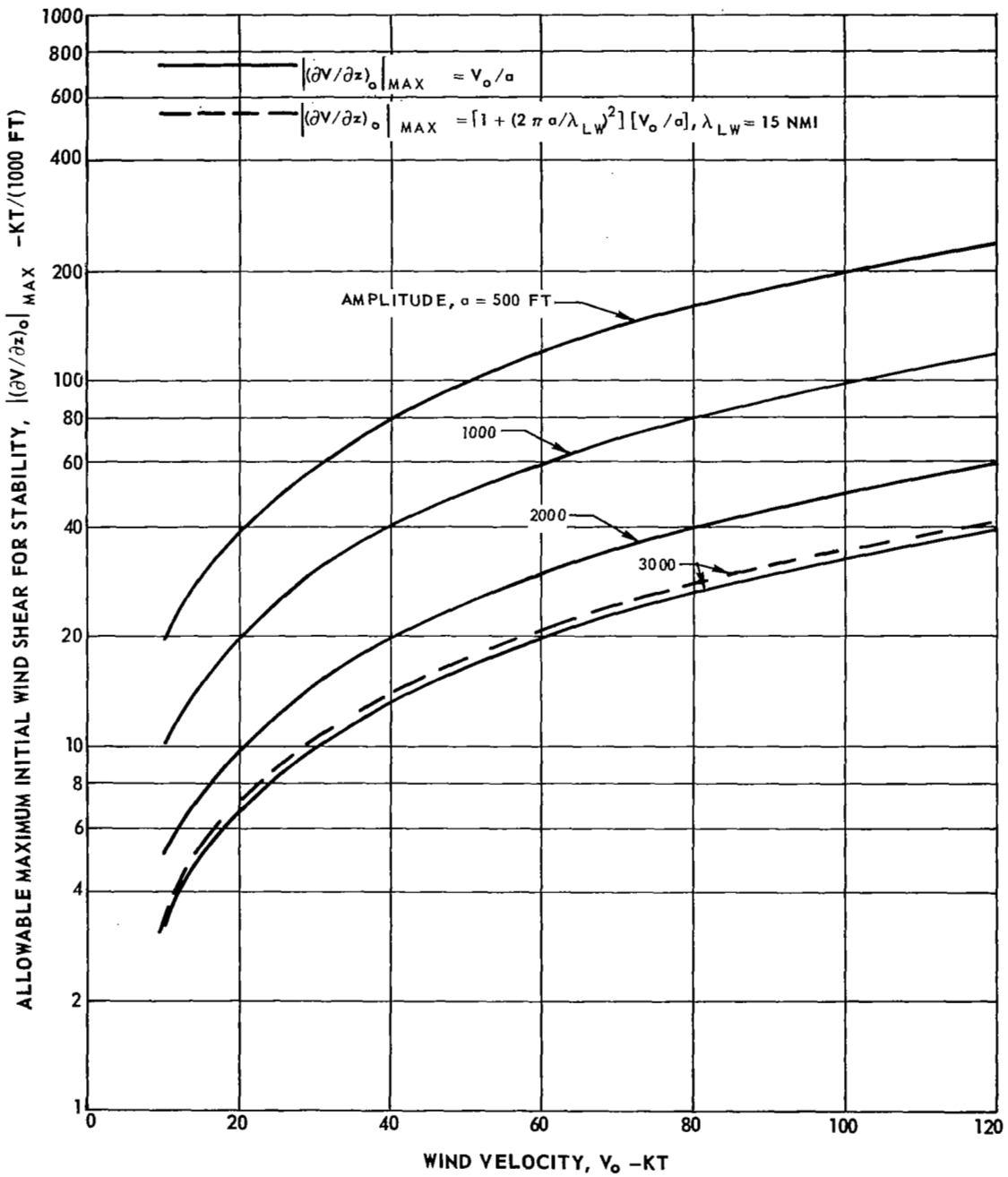

BLOCK DIAGRAM OF COMPUTER PROGRAM FOR PREDICTING WAVE-INDUCED CAT

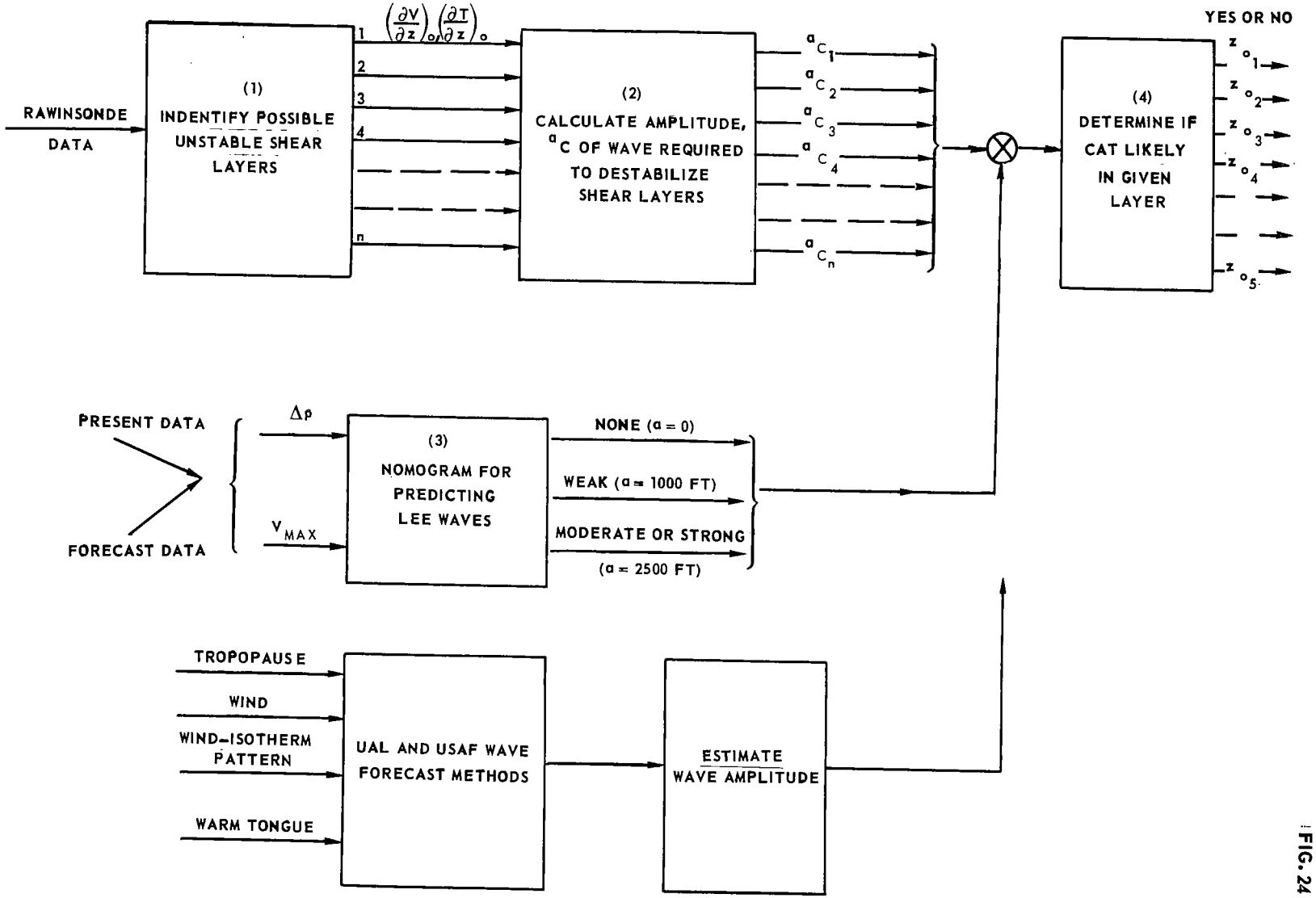

FIG. 24

FIG. 25

COMPARISON OF DATA FROM 1970 LEE WAVE OBSERVATION PROGRAM WITH UNITED AIR LINES NOMOGRAM FOR PREDICTING WAVE OCCURENCE

NOTES: 1. NUMBER NEAR SYMBOL DENOTES FEBRUARY, 1970 DATE
2. NO FLAG DENOTES FLIGHTS NOT MADE AS NO WAVE ACTIVITY WAS PREDICTED BY OTHER METHODS
3. SINGLE FLAG DENOTES WEAK WAVE OBSERVED IN FLIGHT
4. DOUBLE FLAG DENOTES MODERATE WAVE OBSERVED IN FLIGHT

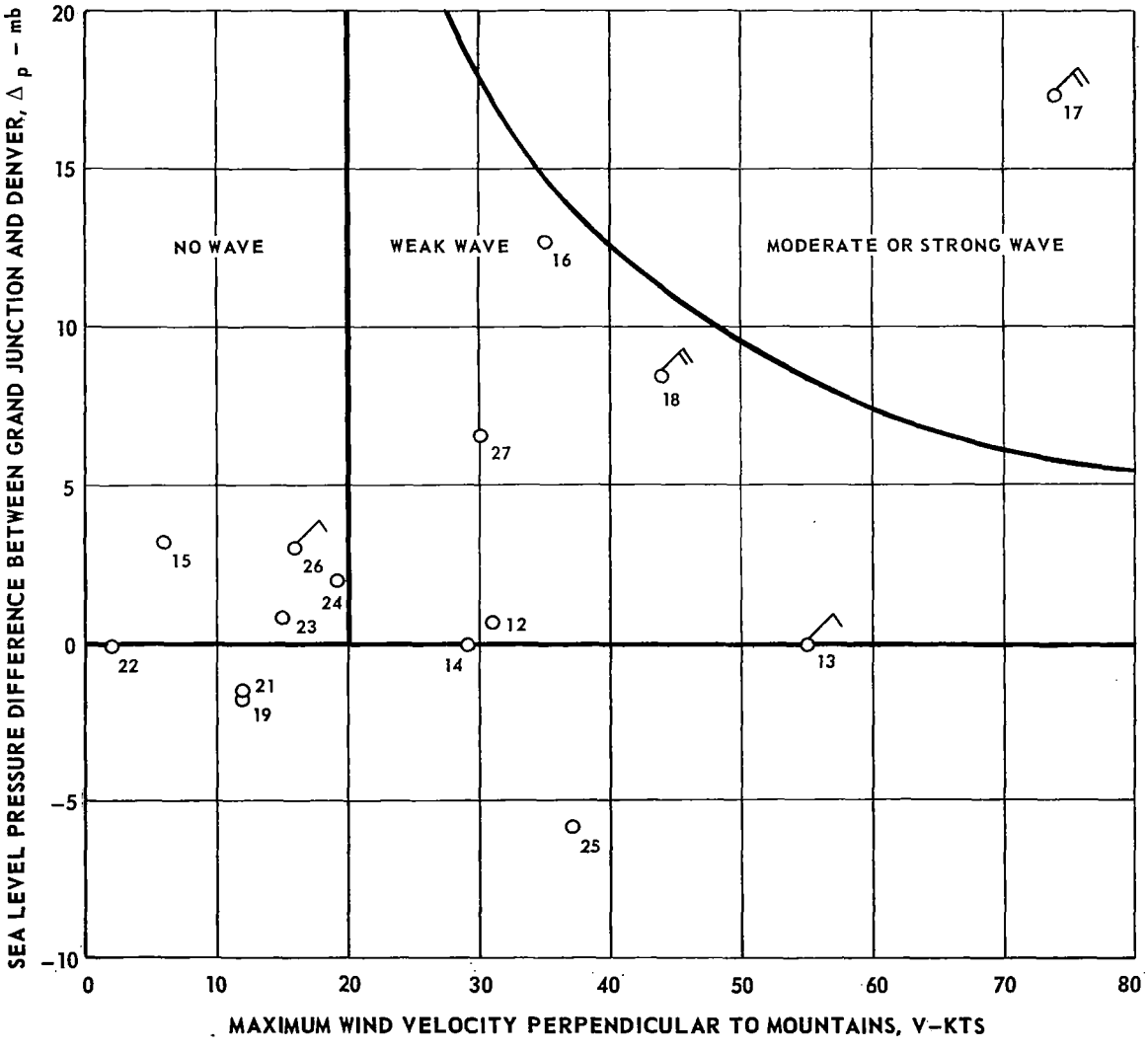

FIG.26

TYPICAL VELOCITY, TEMPERATURE AND DENSITY PROFILES FOR COMBINED SHEAR LAYER EXPERIMENTS

(a) COMBINED LAYER TYPE LARGE–SMALL–LARGE

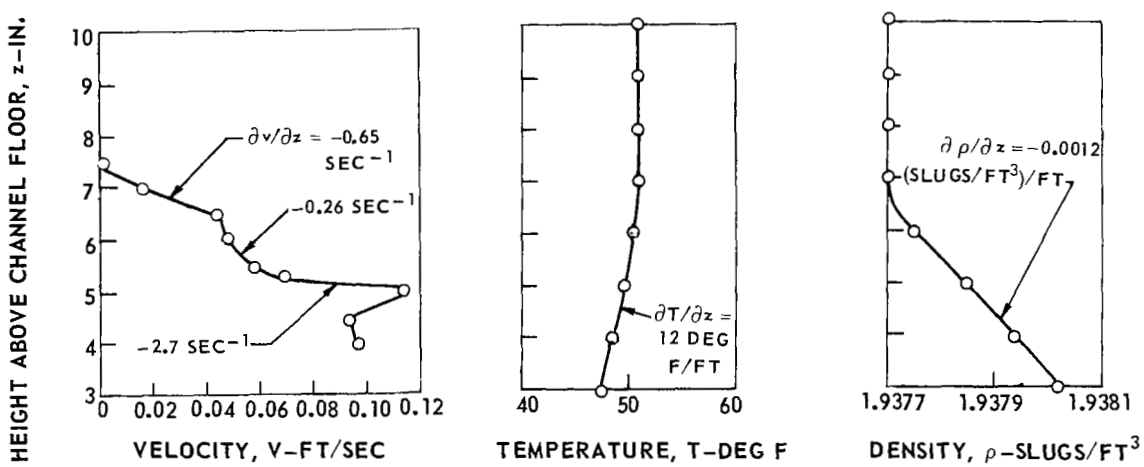

(b) COMBINED LAYER TYPE SMALL– LARGE–SMALL

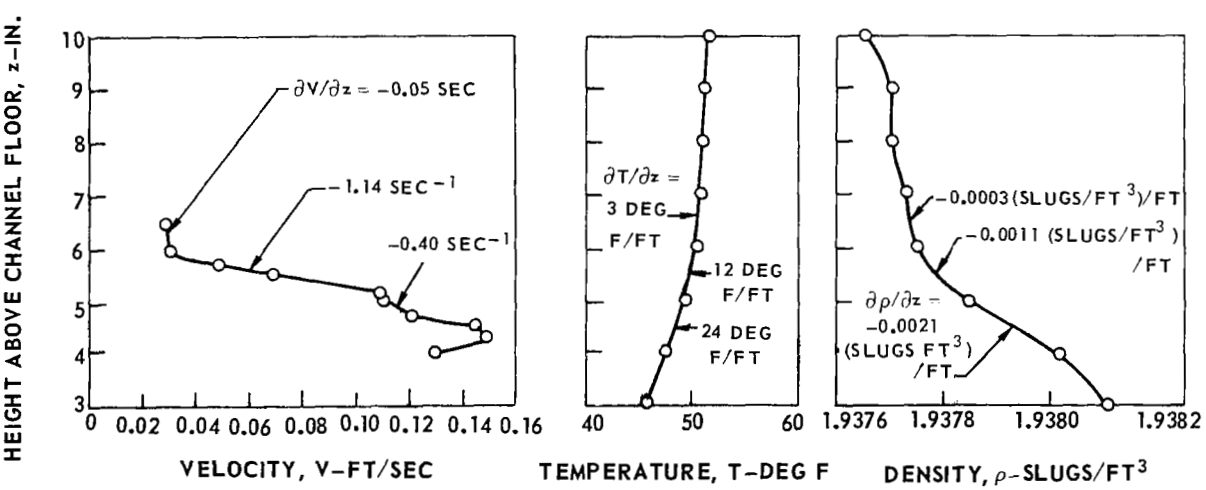

TYPICAL STAGES OF BREAKDOWN OF FLOW IN COMBINED SHEAR LAYERS

(a) COMBINED LAYER TYPE LARGE-SMALL-LARGE

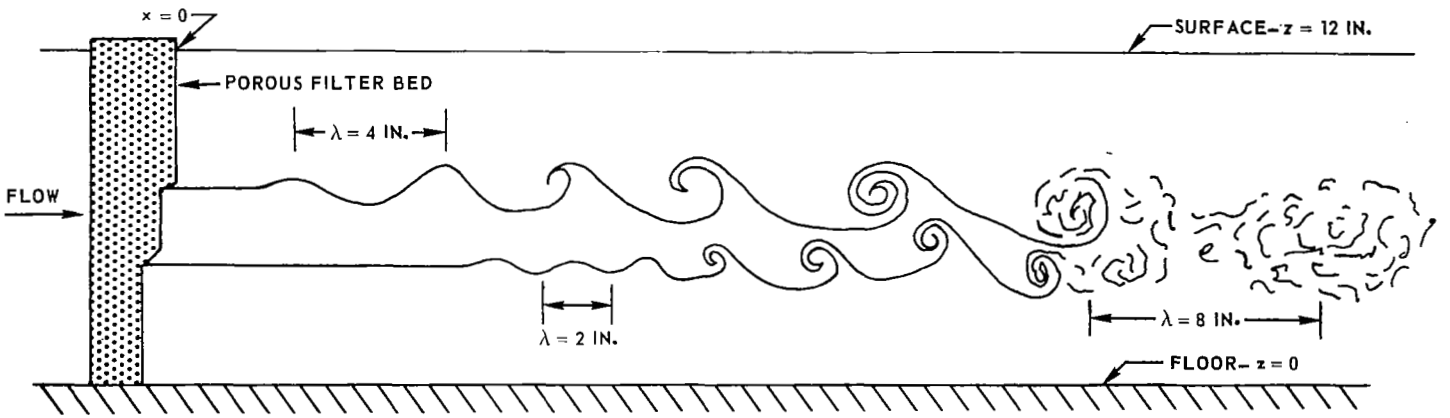

(b) COMBINED LAYER TYPE SMALL-LARGE-SMALL

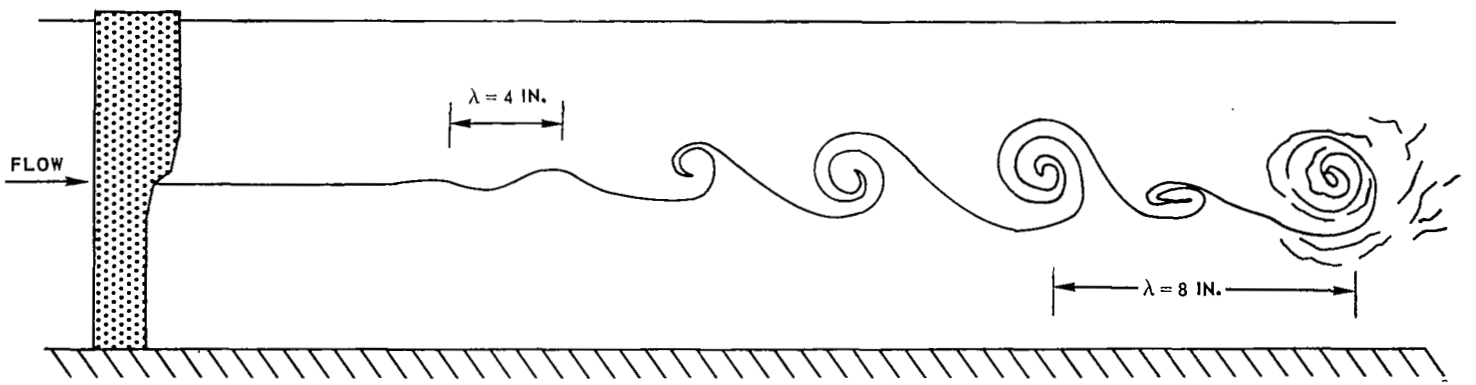

FIG. 27